WATER RESOURCES RESEARCH, VOL. 35, NO. 10, PAGES 2891–2908, OCTOBER 1999

Anisotropy, lacunarity, and upscaled conductivity and its autocovariance in multiscale random fields with truncated power variograms

Vittorio Di Federico

Dipartimento di Ingegneria delle Strutture, dei Transporti, delle Acque, del Rilevamento, del Territorio (DISTART), Università di Bologna, Bologna, Italy

Shlomo P. Neuman

Department of Hydrology and Water Resources, University of Arizona, Tucson

Daniel M. Tartakovsky

Group CIC-19, Los Alamos National Laboratory, Los Alamos, New Mexico

Abstract. It has been shown by *Di Federico and Neuman* [1997, 1998a, b] that observed multiscale behaviors of subsurface fluid flow and transport variables can be explained within the context of a unified stochastic framework, which views hydraulic conductivity as a random fractal characterized by a power variogram. Such a random field is statistically nonhomogeneous but possesses homogeneous spatial increments. *Di Federico and Neuman* [1997] have demonstrated that the power variogram and associated spectra of a statistically isotropic fractal field can be constructed as a weighted integral from zero to infinity (an infinite hierarchy) of exponential or Gaussian variograms and spectra of mutually uncorrelated fields (modes) that are homogeneous and isotropic. We show in this paper that the same holds true when the field and its constituent modes are statistically anisotropic, provided the ratios between principal integral (spatial correlation) scales are the same for all modes. We then analyze the effect of filtering out (truncating) modes of low, high, and intermediate spatial frequency from this infinite hierarchy in the real and spectral domains. A low-frequency cutoff renders the truncated hierarchy homogeneous. The integral scales of the lowest- and highest-frequency cutoff modes are related to length scales of the sampling window (domain) and data support (sample volume), respectively. Taking the former to be proportional to the latter renders expressions for the integral scale and variance of the truncated field dependent on window and support scale (in a manner previously shown to be consistent with observations in the isotropic case). It also allows (in principle) bridging across scales at a specific locale, as well as among locales, by adopting either site-specific or generalized variogram parameters. The introduction of intermediate cutoffs allows us to account, in a straightforward manner, for lacunarity due to gaps in the multiscale hierarchy created by the absence of modes associated with discrete ranges of scales (for example, where textural and structural features are associated with distinct ranges of scale, such as fractures having discrete ranges of trace length and density, which dissect the rock into matrix blocks having corresponding ranges of sizes). We explore mathematically and graphically the effects that anisotropy and lacunarity have on the integral scale, variance, covariance, and spectra of a truncated fractal field. We then develop an expression for the equivalent hydraulic conductivity of a box-shaped porous block, embedded within a multiscale log hydraulic conductivity field, under mean-uniform flow. The block is larger than the support scale of the field but is smaller than a surrounding sampling window. Consequently, its equivalent hydraulic conductivity is a random variable whose variance and spatial autocorrelation function, conditioned on a known mean value of support-scale conductivity across the window, are given explicitly by our multiscale theory.

1. Introduction

Geologic media are heterogeneous and exhibit both discrete and continuous spatial variations on a multiplicity of scales. It is therefore not surprising that the same is true of their flow and transport properties. One manifestation of multiscale heterogeneity is the apparent increase in spatial correlation scale and variance of natural log hydraulic conductivity $Y = \ln K$ with the size of the domain under investigation; another is the apparent dependence of permeabilities and dispersivities on their scale of measurement or observation [*Neuman and Di Federico*, 1998]. A scaling theory that establishes a consistent link between these phenomena has recently been advanced by

Paper number 1999WR900158.
0043-1397/99/1999WR900158$09.00

Di Federico and Neuman [1997, 1998a, b; see also *Neuman and Di Federico*, 1998]. It rests on the observation that at an increasing number of sites on distance scales ranging from a few meters to 100 km [*Grindrod and Impey*, 1992; *Desbarats and Bachu*, 1994; *Molz and Boman*, 1995; *Guzman and Neuman*, 1996; *Liu and Molz*, 1996], $Y(\mathbf{x})$ data appear to represent a nonstationary field with homogeneous spatial increments. When this field is statistically isotropic, it is associated with a power variogram $\gamma(s) = as^{2H}$, where a is a constant, s is separation distance, and H is a Hurst coefficient. Since the variogram scales as $\gamma(rs) = r^{2H}\gamma(s)$, the field is self-affine and within the range $0 < H < 1$ constitutes a random fractal with dimension $D = d + 1 - H$, where d is Euclidean (topologic) dimension [*Voss*, 1985]. If the field is additionally Gaussian, it constitutes fractional Brownian motion (fBm) [*Mandelbrot and Van Ness*, 1968]. When $0.5 < H < 1$, random spatial increments in field values are positively correlated so that positive and negative deviations from the mean tend to persist over distance, a phenomenon known as persistence. When $0 < H < 0.5$, the increments are negatively correlated so that positive and negative deviations from the mean tend to alternate rapidly, a phenomenon called antipersistence. When $H = 0.5$, the increments are uncorrelated and the field represents Brownian motion.

The Hurst coefficient associated with an fBm description of Y is not the same at each site, though it has been found to lie near the midrange of $0 < H < 0.5$ in most of the above studies, some of which emphasize horizontal and some of which emphasize vertical variations in Y (*Ababou and Gelhar* [1990] work with $H \approx 0$, while *Aasum et al*. [1991] find $H > 0.5$). Within this range the increments are negatively correlated and relatively noisy, exhibiting antipersistent behavior. Nevertheless, when one juxtaposes apparent values of variance and integral scale from many sites, inferred from Y data by assuming that the underlying field is homogeneous, one finds that they fit a generalized power model with $H \approx 0.25$ [*Neuman*, 1994]. Such generalized behavior has been deduced earlier by *Neuman* [1990] from the observed scale dependence of juxtaposed apparent dispersivities reported for a large number of tracer studies worldwide.

Though one can represent multiscale random heterogeneity by means of other models, such as fractional Gaussian noise (fGn) [*Robin et al*., 1991; *Molz and Boman*, 1993, 1995; *Tubman and Crane*, 1995; *Eggleston and Rojstaczer*, 1998] (these studies typically yield $H > 0.5$), corresponding power law approximations [*Glimm et al*., 1993; *Dagan*, 1994], Weierstrass-Mandelbrot fractal function [*Molz et al*., 1998], fractional Levy motion (fLm) [*Painter*, 1996a, b], or multifractals [*Liu and Molz*, 1997; *Molz et al*., 1997], their reliance on fBm allowed *Di Federico and Neuman* [1997] to establish a geostatistical framework within which they had been able to solve multiscale flow and transport problems by well-established methods of stochastic analysis [*Di Federico and Neuman*, 1998a, b]. The geostatistical framework rests on a discovery by *Neuman* [1990] and *Di Federico and Neuman* [1997] that the variogram and spectra of fBm can be constructed as, or decomposed into, an infinite hierarchy of either exponential or Gaussian variograms and spectra of mutually uncorrelated, statistically homogeneous and isotropic random fields (modes). Filtering out (truncating) low-frequency (large scale) modes from this infinite hierarchy renders it statistically homogeneous with a positive spatial autocovariance function that decays monotonically with separation distance in a manner not too dissimilar from that of its constituent (exponential or Gaussian) modes. The integral scale λ_l of the low-frequency cutoff mode is related to the length scale of a sampling window defined by the region under investigation. If a high-frequency (small scale) cutoff is present, then its integral scale λ_u is related to the length scale of data support (volume of measurement). Taking each relationship to be one of proportionality renders the integral scale and variance of a truncated field dependent on window and support scales in a manner consistent with observations.

The multiscale geostatistical framework of *Di Federico and Neuman* [1997] allows bridging across scales at a given locale by calibrating a truncated variogram model to data observed on a given support in one domain and predicting the autocovariance structure of the corresponding field in domains that are either smaller or larger. One may also venture bridging across both domain scales and locales by using generalized parameters such as $H \approx 0.25$, derived on the basis of juxtaposed data from many sites.

The geostatistical theory of *Di Federico and Neuman* [1997] allowed *Di Federico and Neuman* [1998a] to investigate analytically, by means of a standard perturbation method, mean-uniform steady state groundwater flow in unbounded, two- and three-dimensional domains where the log hydraulic conductivity forms a truncated multiscale hierarchy of Gaussian fields, each associated with an exponential autocovariance. They started by deriving an expression for effective hydraulic conductivity, as a function of the Hurst coefficient H and the cutoff scales in one-, two-, and three-dimensional domains, which is qualitatively consistent with observed variations in hydraulic conductivity with the scale of measurement. They then developed leading-order analytical expressions for two- and three-dimensional autocovariance and cross-covariance functions of hydraulic head, velocity, and log hydraulic conductivity versus H, λ_l, and λ_u, examined their behavior, and compared them with those corresponding to an exponential log hydraulic conductivity autocovariance. Their results suggested that it should be possible to bridge information about hydraulic heads and groundwater velocities across windows of disparate scales. In particular, they found that when $\lambda_l \gg \lambda_u$, the variance of head is infinite in two dimensions and grows in proportion to λ_l^{2+2H} in three dimensions, while the variance and longitudinal integral scale of velocity grow in proportion to λ_l^{2H} and λ_l, respectively, in both cases.

The latter work formed the basis for a subsequent perturbation analysis by *Di Federico and Neuman* [1998b] of advective transport in a multiscale velocity field. They found that if one considers such transport to be affected by a finite domain much larger than the mean travel distance of a plume, so that $s \ll \lambda_l < \infty$, then an early preasymptotic regime develops during which longitudinal and transverse dispersivities grow linearly with s. If one considers transport to be affected by a domain which increases in proportion to s, then λ_l and s are of similar order and a preasymptotic regime never develops. Instead, transport occurs under a regime that is perpetually close to asymptotic under the control of an evolving scale, $\lambda_l \sim s$. They showed that if, additionally, $\lambda_u \ll \lambda_l$, then the corresponding longitudinal dispersivity grows in proportion to λ_l^{1+2H} or, equivalently, s^{1+2H}. Both these preasymptotic and asymptotic theoretical growth rates are consistent with the observed variation of apparent longitudinal Fickian dispersivities with scale. The authors concluded their analysis by inves-

tigating the effect of variable separations between cutoff scales on dispersion.

The log hydraulic conductivity of many geologic media exhibits statistical anisotropy [*Hufschmied*, 1985; *Sudicky*, 1986; *Neuman and Depner*, 1988]. *Hewett* [1992], *Molz and Boman* [1993], *Perez and Kalkar* [1993], and *Molz et al*. [1998] represented anisotropy through a combination of vertical fGn and horizontal fBm models having identical Hurst coefficients; *Rajaram and Gelhar* [1995] and *Zhan and Wheatcraft* [1996] introduced anisotropy into power spectra of fGn and/or fBm. In this paper we extend the geostatistical framework of *Di Federico and Neuman* [1997] to the case of a nonhomogeneous random field that possesses homogeneous but anisotropic spatial increments. We demonstrate that the power variogram and associated spectra of such a field can be constructed as weighted integrals from zero to infinity of variograms and spectra of mutually uncorrelated, statistically homogeneous but anisotropic random fields, or modes, with either exponential or Gaussian variograms, all of which have identical anisotropy ratios. We then analyze the effect of filtering out (truncating) high- and low-frequency modes from this infinite hierarchy in the real and spectral domains. Our analysis shows that, as in the isotropic case, a low-frequency cutoff renders the truncated hierarchy statistically homogeneous with an anisotropic spatial autocovariance that varies monotonically with separation distance in a manner not too dissimilar from that of its constituent modes.

By introducing intermediate cutoffs, we find it possible to account for gaps in the multiscale hierarchy created by the absence of modes associated with discrete ranges of scales, a phenomenon which we refer to as lacunarity. It is easy to think of examples in which textural, structural, petrophysical, hydrological, or other features and attributes of a geologic medium are associated with discrete ranges of scales rather than with an uninterrupted continuum of such scales. One such example is provided by fractures having discrete ranges of trace length and density, which dissect the rock into matrix blocks having corresponding ranges of sizes. In such a fractured-porous environment the spatial autocorrelation scale of matrix log conductivity is often small in comparison to the shortest scale associated with fracture conductivity, so that there is a gap between the two sets of scales. We refer to such gaps as lacunae and to the corresponding phenomenon as lacunarity. Our use of the term differs from that of *Mandelbrot* [1983], who used it to connote gaps or holes in the geometric image of a fractal object. The need to consider lacunarity in the context of multiscale log conductivity fields was recently pointed out by *Liu and Molz* [1998] and *Molz et al*. [1998]. We explore mathematically and graphically the effects that anisotropy and lacunarity have on the integral scale, variance, covariance, and spectra of a truncated anisotropic fractal field.

Finally, we develop an expression for the equivalent hydraulic conductivity of a box-shaped porous block, embedded within a multiscale log hydraulic conductivity field, under mean-uniform flow. The block is larger than the support scale of the field but is smaller than a surrounding sampling window. Consequently, its equivalent hydraulic conductivity is a random variable whose variance and spatial autocorrelation function, conditioned on a known mean value of support-scale conductivity across the window, are given explicitly by our multiscale theory.

2. Anisotropic Multiscale Random Fields as Superposition of Mutually Uncorrelated Modes

2.1. Superposition of Modes in Real Domain

It is common practice [i.e., *Neuman and Depner*, 1988] to treat anisotropic covariance functions as being elliptical. This means that in the anisotropic domain one can define a system of principal Cartesian coordinates $\mathbf{x}$, and corresponding principal spatial autocorrelation or integral scales λ, λ_2, and λ_3, such that the covariance becomes isotropic when $\mathbf{x}$ is transformed according to

$$\mathbf{x}^* = \boldsymbol{\delta}^{-1}\mathbf{x} \tag{1}$$

where

$$\boldsymbol{\delta} = \begin{pmatrix} 1 & 0 & 0 \\ 0 & e_2 & 0 \\ 0 & 0 & e_3 \end{pmatrix} \qquad e_2 = \lambda_2/\lambda \qquad e_3 = \lambda_3/\lambda \tag{2}$$

Consider an infinite hierarchy of mutually uncorrelated, statistically homogeneous, and anisotropic random fields (modes), each of which is associated with an exponential or Gaussian variogram

$$\gamma(\mathbf{s}, \lambda, \lambda_2, \lambda_3) = \sigma^2(\lambda)\left\{1 - \exp\left[-\left(\frac{s_1^2}{\lambda^2} + \frac{s_2^2}{\lambda_2^2} + \frac{s_3^2}{\lambda_3^2}\right)^{1/2}\right]\right\} \tag{3}$$

$$\gamma(\mathbf{s}, \lambda, \lambda_2, \lambda_3) = \sigma^2(\lambda)\left\{1 - \exp\left[-\frac{\pi}{4}\left(\frac{s_1^2}{\lambda^2} + \frac{s_2^2}{\lambda_2^2} + \frac{s_3^2}{\lambda_3^2}\right)\right]\right\} \tag{4}$$

where

$$\sigma^2(n) = C/n^{2H} \tag{5}$$

$\mathbf{s}$ is a separation vector, C is a constant having dimensions $[L^{-2H}]$, and $n = 1/\lambda$ is a principal mode number, so that the variance decreases as a power $2H$ of this number. The variograms in (3) and (4) can be rewritten in terms of transformed separation distances as

$$\gamma(\mathbf{s}^*, \lambda, e_2, e_3) = \sigma^2(\lambda)\left[1 - \exp\left(-\frac{s^*}{\lambda}\right)\right] \tag{6}$$

$$\gamma(\mathbf{s}^*, \lambda, e_2, e_3) = \sigma^2(\lambda)\left[1 - \exp\left(-\frac{\pi s^{*2}}{4\lambda^2}\right)\right] \tag{7}$$

where

$$s^* = |\mathbf{s}^*| = s(\mathbf{u}^T\boldsymbol{\delta}^{-2}\mathbf{u})^{1/2} \tag{8}$$

$s = |\mathbf{s}|$, $\mathbf{u}$ is a unit vector parallel to a given direction in the original anisotropic system of coordinates, and the superscript T indicates transpose. Let the anisotropy ratios e_2 and e_3 be independent of mode number n and consider the weighted integral

$$\gamma(s^*) = \int_0^\infty \gamma(s^*, n)\,\frac{dn}{n} \tag{9}$$

of variograms of individual modes over the entire admissible range of scales. Since the variograms γ are expressed in terms of s^*, they do not depend explicitly on e_2 and e_3. This equation is identical in form to (11) of *Di Federico and Neuman* [1997]. Upon substituting (5) into (6) or (7) and substituting

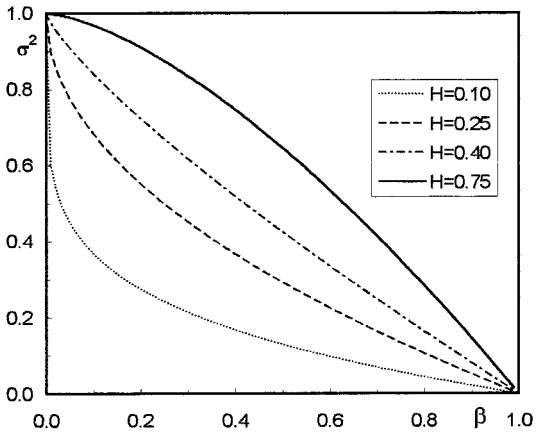

Figure 1. Dimensionless variance versus β for various H.

these into (9), one immediately finds in analogy to (12) and (25) of *Di Federico and Neuman* [1997] that

$$\gamma(s^*) = C_0 s^{*2H} \tag{10}$$

$$\gamma(s^*) = C_0' s^{*2H} \tag{11}$$

for exponential and Gaussian modes, respectively, which transform into

$$\gamma(\mathbf{s}) = C_0\left(s_1^2 + \frac{s_2^2}{e_2^2} + \frac{s_3^2}{e_3^2}\right)^H \tag{12}$$

$$\gamma(\mathbf{s}) = C_0'\left(s_1^2 + \frac{s_2^2}{e_2^2} + \frac{s_3^2}{e_3^2}\right)^H \tag{13}$$

where

$$C_0 = C\,\frac{\Gamma(1-2H)}{2H} \qquad 0 < H < 1/2 \tag{14}$$

$$C_0' = C\,\frac{\Gamma(1-H)}{2H}\left(\frac{\pi}{4}\right)^H \qquad 0 < H < 1 \tag{15}$$

are constants proportional to C having the same dimensions and Γ is the gamma function. The above implies that any power variogram of the form (12) or (13) can be constructed mathematically as (or decomposed into) a nonunique weighted sum of mutually uncorrelated exponential or Gaussian anisotropic modes.

Consider now the case

$$\gamma(s^*, n_l, n_u) = \int_{n_l}^{n_u} \gamma(s^*, n)\,\frac{dn}{n} \tag{16}$$

where integration is performed with lower and upper cutoffs $n_l = 1/\lambda_l$ and $n_u = 1/\lambda_u$, so that all modes with integral scale larger than λ_l and lower than λ_u are filtered out (excluded). As indicated by *Di Federico and Neuman* [1997], the integral scales of the lowest- and highest-frequency cutoff modes are related to the length scales of the sampling window (domain) and data support (sample volume), respectively. As we take the cutoffs in (16) to apply equally along all three (principal) coordinate directions, they delineate a cubic window and support volume in the equivalent isotropic domain of s^*, which, in turn, attain brick shapes upon back transformation into the corresponding anisotropic coordinates. Then, in analogy to (20) of *Di Federico and Neuman* [1997],

$$\gamma(s^*, n_l, n_u) = \gamma(s^*, n_l) - \gamma(s^*, n_u) \tag{17}$$

where according to their (15) and (27)

$$\gamma(s^*, n_m) = \frac{C_0}{\Gamma(1-2H)n_m^{2H}}\left[1 - \exp(-n_m s^*) + (n_m s^*)^{2H}\Gamma(1-2H, n_m s^*)\right] \tag{18}$$

$$\gamma(s^*, n_m) = \frac{C_0'}{\Gamma(1-H)(\pi/4)^H n_m^{2H}}\left[1 - \exp\left(-\frac{\pi}{4}n_m^2 s^{*2}\right) + \left(\frac{\pi}{4}n_m^2 s^{*2}\right)^H \Gamma\left(1-H, \frac{\pi}{4}n_m^2 s^{*2}\right)\right] \tag{19}$$

for exponential and Gaussian modes, respectively. In (18) and (19), $m = l, u$ and $\Gamma(a, x)$ is the incomplete gamma function; in the limit as $n_l \to 0$ and $n_u \to \infty$, (17) reduces to (10) or (11), depending on mode type. The variogram (17) defines a homogeneous field associated with a constant variance

$$\sigma^2(n_l, n_u) = \sigma^2(n_l) - \sigma^2(n_u) \tag{20}$$

autocovariance $C(s^*, n_l, n_u) = \sigma^2(n_l, n_u) - \gamma(s^*, n_l, n_u)$ given by

$$C(s^*, n_l, n_u) = C(s^*, n_l) - C(s^*, n_u) \tag{21}$$

and finite integral scale

$$I(n_l, n_u, \mathbf{u}) = \frac{2H}{1+2H}\,\frac{n_u^{1+2H} - n_l^{1+2H}}{n_l n_u (n_u^{2H} - n_l^{2H})}\,(\mathbf{u}^T\boldsymbol{\delta}^{-2}\mathbf{u})^{1/2} \tag{22}$$

where

$$\sigma^2(n_m) = \frac{C_0}{\Gamma(1-2H)n_m^{2H}} \tag{23}$$

$$C(s^*, n_m) = \frac{C_0}{\Gamma(1-2H)n_m^{2H}} \cdot [\exp(-n_m s^*) - (n_m s^*)^{2H}\Gamma(1-2H, n_m s^*)] \tag{24}$$

for exponential modes, and

$$\sigma^2(n_m) = \frac{C_0'}{\Gamma(1-H)(\pi/4)^H n_m^{2H}} \tag{25}$$

$$C(s^*, n_m) = \frac{C_0'}{\Gamma(1-H)(\pi/4)^H n_m^{2H}} \cdot \left[\exp\left(-\frac{\pi}{4}n_m^2 s^{*2}\right) - \left(\frac{\pi}{4}n_m^2 s^{*2}\right)^H \Gamma\left(1-H, \frac{\pi}{4}n_m^2 s^{*2}\right)\right] \tag{26}$$

for Gaussian modes. In the absence of a high-frequency cutoff where $n_u \to \infty$, (22) simplifies to

$$I(n_l, \mathbf{u}) = \frac{2H}{1+2H}\,\frac{1}{n_l}\,(\mathbf{u}^T\boldsymbol{\delta}^{-2}\mathbf{u})^{1/2} \tag{27}$$

The above equations reduce to their isotropic analogues in the work of *Di Federico and Neuman* [1997] when $e_2 = e_3 = 1$.

We introduce the cutoff ratio $\beta = n_l/n_u$, $0 \le \beta \le 1$ and $n_l > 0$ and show in Figure 1 the variance given in (20), normalized with respect to its value at $\beta = 0$, as a function of

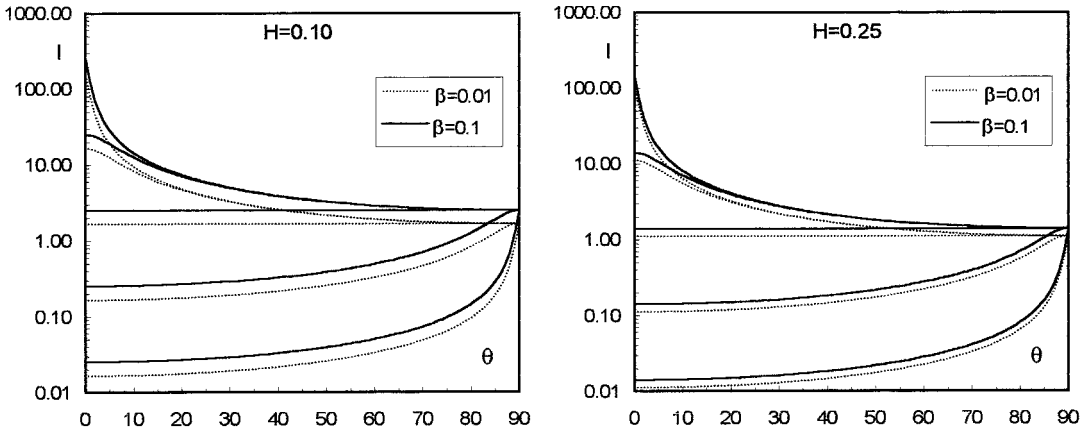

Figure 2. Dimensionless integral scale versus angle θ for various e (from bottom to top, $e = 0.01, 0.1, 1, 10,$ and 100), β, and H.

β for $H = 0.10, 0.25, 0.40, 0.75$, where the case $H = 0.75$ represents only Gaussian modes. Since here we take $n_l > 0$, the case $\beta = 0$ represents absence of an upper cutoff (in practice, an upper cutoff scale and corresponding support scale that are small compared to the scales of the lower cutoff and window). The normalized variance is seen to decrease as β increases and to diminish as H becomes small. In many practical applications, $\beta < 0.01$, and the reduction in variance is modest. The integral scale in (22) depends on the direction of the unit vector **u**. We let θ designate the angle between **u** and the vertical and normalize the integral scale with respect to its horizontal ($\theta = 90°$) value at $\beta = 0$. Figure 2 shows how this normalized integral scale varies with θ for various values of H, β, and the axisymmetric anisotropy ratio e which takes on, from bottom to top, the values 0.01, 0.1, 1, 10, and 100. When $e < 1$ so that the spatial autocorrelation scales of each mode are larger in the horizontal than in the vertical direction, the normalized integral scale of the truncated hierarchy increases with θ; it decreases with θ when $e > 1$. In the isotropic case where $e = 1$, the normalized integral scale of the hierarchy does not vary with θ. In all cases it increases with β and decreases with H.

The autocorrelation function $\rho(s, n_l) = C(s, n_l)/\sigma^2(n_l)$ corresponding to exponential and Gaussian modes without an upper cutoff ($\beta = 0$) and with axisymmetric statistical anisotropy ($e_2 = 1$ and $e_3 = e$) is plotted in Figures 3 and 4, respectively. Figures 3 and 4 show how these functions vary with dimensionless distance $n_l s$, along various directions defined by the angles θ and ϕ between **u** and the coordinates x_3 and x_1, respectively, for various values of e and H. The left columns in Figures 3 and 4 depict vertical ($\theta = 0°$, any ϕ) and the second intermediate ($\theta = 45°$, $\phi = 45°$) autocorrelation functions; curves corresponding to $e = 1$ in either left or right columns coincide with the horizontal autocorrelation functions. In both columns the autocorrelation functions are seen to increase with e and H. When $e > 1$, these functions decay more slowly in the vertical than in the intermediate direction; curves corresponding to $e = 10$ and 100 in this latter direction are virtually indistinguishable from each other. Autocorrelation functions corresponding to exponential and Gaussian modes are quite similar to each other within their joint range of admissible Hurst coefficients, $0 < H < 0.5$, but the latter decay more slowly near the origin outside of this range, where $H > 0.50$.

Figure 5 shows how the introduction of an upper cutoff affects multiscale autocorrelation functions $\rho(s, n_l, n_u) = C(s, n_l, n_u)/\sigma^2(n_l, n_u)$ that represent sums of exponential modes. The functions are plotted versus $n_l s$ for various anisotropy ratios e (which takes on, from bottom to top, the values 0.01, 0.1, 1, 10, and 100), $H = 0.25$, two values of β (0.01 and 0.1), and two directions (vertical with $\theta = 0°$ and any ϕ and intermediate with $\theta = 45°$ and $\phi = 45°$). As β (i.e., the smaller cutoff scale relative to the larger one) increases, the autocorrelation is seen to become more pronounced and to decay more slowly.

2.2. Superposition of Modes in Spectral Domain

All results obtained in the real domain have a direct counterpart in the spectral domain. In the equivalent isotropic domain the spectral density and autocovariance are related through the Fourier transform pair

$$S(\mathbf{k}^*) = \frac{1}{(2\pi)^d} \int_{-\infty}^{\infty} C(\mathbf{s}^*) e^{-i\mathbf{k}^*\cdot\mathbf{s}^*}\, d\mathbf{s}^* \tag{28}$$

$$C(\mathbf{s}^*) = \int_{-\infty}^{+\infty} S(\mathbf{k}^*) e^{i\mathbf{k}^*\cdot\mathbf{s}^*}\, d\mathbf{k}^* \tag{29}$$

where $\mathbf{k}^*$ is a vector of wave numbers. Defining a corresponding vector $\mathbf{k}$ in the principal coordinates according to

$$\mathbf{k}^* = \boldsymbol{\delta}\mathbf{k} \tag{30}$$

where $\boldsymbol{\delta}$ was defined in (2), we find in analogy to (33) and (38) of *Di Federico and Neuman* [1997] that the three-dimensional spectral densities associated with exponential and Gaussian anisotropic modes become

$$S(\mathbf{k}, \lambda, \lambda_2, \lambda_3) = \frac{\sigma^2(\lambda)\lambda\lambda_2\lambda_3}{\pi^2(1 + k_1^2\lambda^2 + k_2^2\lambda_2^2 + k_3^2\lambda_3^2)^2} \tag{31}$$

$$S(\mathbf{k}, \lambda, \lambda_2, \lambda_3) = \frac{\sigma^2(\lambda)\lambda\lambda_2\lambda_3}{\pi^3} \exp\left[-\frac{1}{\pi} (k_1^2\lambda^2 + k_2^2\lambda_2^2 + k_3^2\lambda_3^2) \right] \tag{32}$$

respectively. Upon setting $\lambda = 1/n$, the superposition of a continuous hierarchy of individual spectra over all possible scales, weighted by $1/n$, is accomplished in the equivalent isotropic domain via

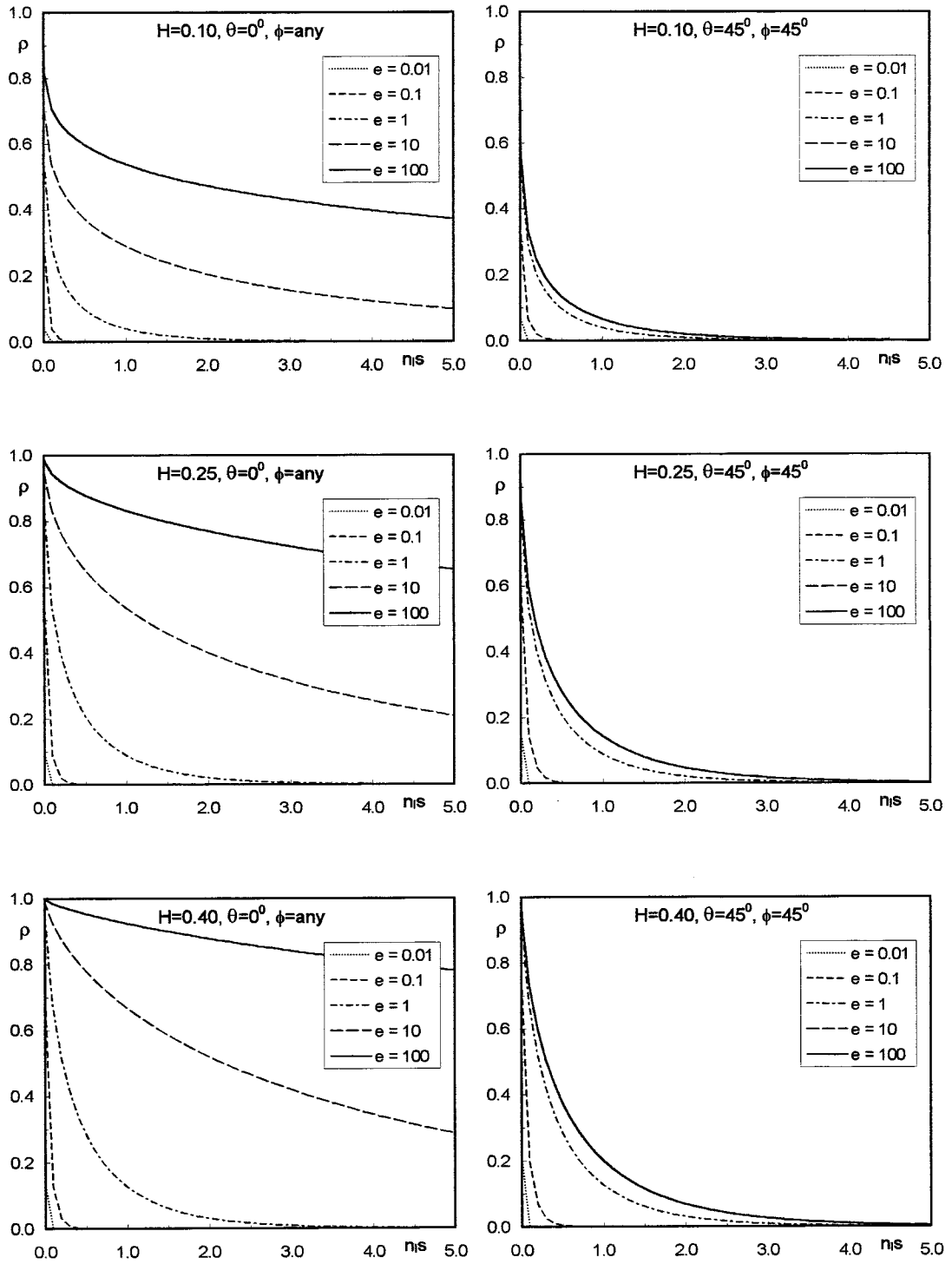

Figure 3. Autocorrelation function corresponding to anisotropic exponential modes with low-frequency cutoff versus dimensionless distance $n_l s$ for various e, H, and directional angles θ and ϕ.

$$S(k^*) = \int_0^\infty S(k^*, n)\,\frac{dn}{n} \tag{33}$$

where $k^* = |\mathbf{k}^*|$. Defining the variance in (31) and (32) according to (5) and integrating these equations according to (33) yields, in analogy to (35) of *Di Federico and Neuman* [1997], the following spectral densities for superimposed exponential and Gaussian modes in the anisotropic domain:

$$S(\mathbf{k}) = \frac{C_0 e_2 e_3 (1 + 2H)\Gamma(1 + 2H)}{2\pi\Gamma(H)\Gamma(1 - H)(k_1^2 + e_2^2 k_2^2 + e_3^2 k_3^2)^{(3+2H)/2}} \tag{34}$$

$$S(\mathbf{k}) = \frac{C_0' e_2 e_3 (1 + 2H)\Gamma(1 + 2H)}{2\pi\Gamma(H)\Gamma(1 - H)(k_1^2 + e_2^2 k_2^2 + e_3^2 k_3^2)^{(3+2H)/2}} \tag{35}$$

respectively, which are valid over the respective ranges $0 < H < \frac{1}{2}$ and $0 < H < 1$. These spectral densities correspond

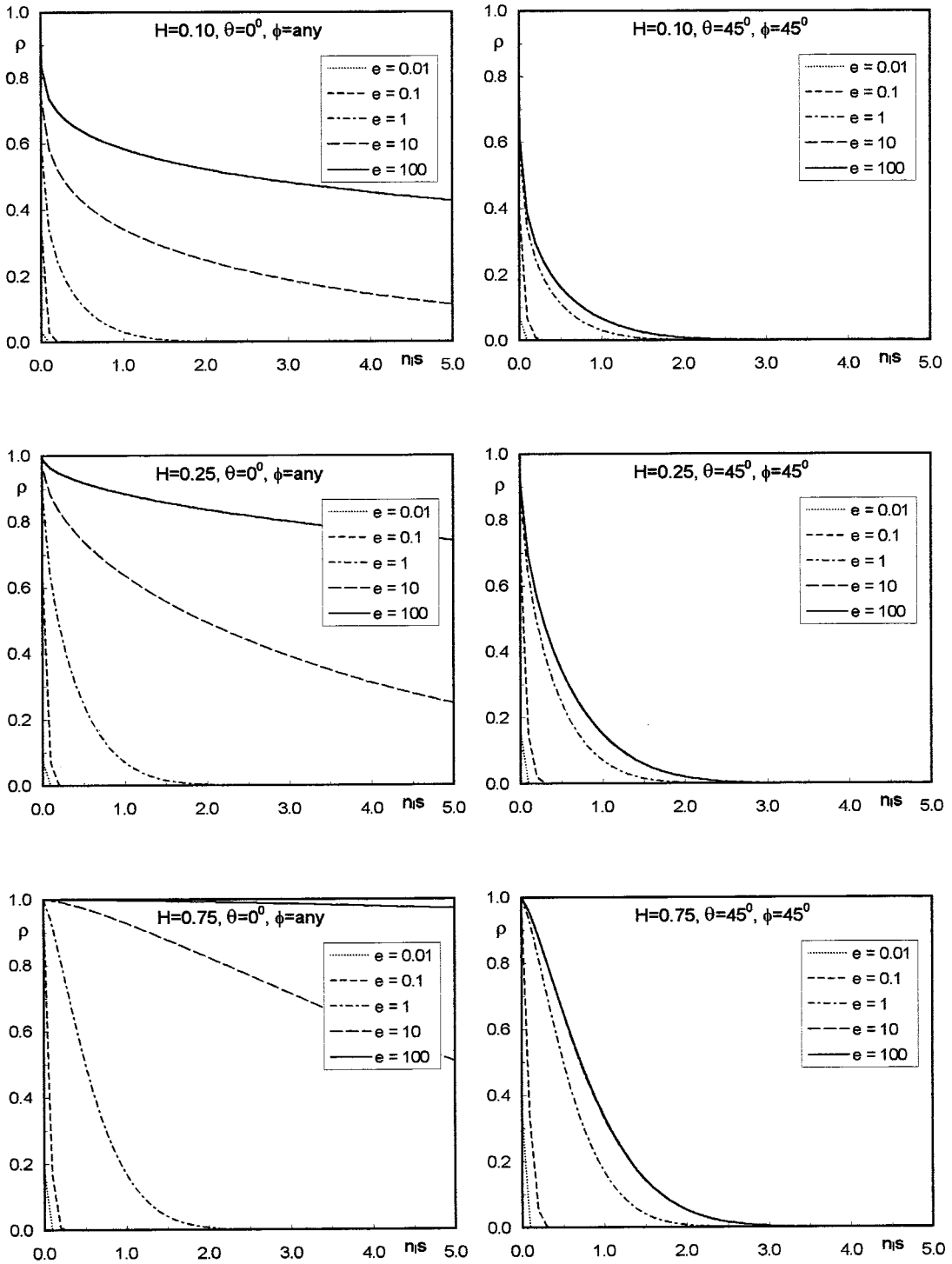

Figure 4. Same as Figure 3 but corresponding to anisotropic Gaussian modes.

exactly to variograms (6) and (7), respectively, thus demonstrating that our weighted superposition leads to identical results in the real and in spectral domains.

Rajaram and Gelhar [1995, equation (13)] postulated the following form for the spectral density of a three-dimensional fBm with vertical to horizontal (axisymmetric) anisotropy ratio e,

$$S(\mathbf{k}) = \frac{c}{(k_1^2 + k_2^2 + e^2 k_3^2)^{(m+3)/2}} \tag{36}$$

where c and m are constants. This intuitive spectrum becomes identical to our formally derived (34) and (35) provided that one sets $m = 2H$, $e_2 = 1$, $e_3 = e$, and c equal to the corresponding coefficient of (34) or (35).

Introducing lower and upper cutoffs by setting the lower and upper limits of integration in (33) equal to n_l and n_u, respectively, leads in analogy to (37), (36), and (39) of *Di Federico and Neuman* [1997] to

$$S(k^*, n_l, n_u) = S(k^*, n_l) - S(k^*, n_u) \tag{37}$$

where

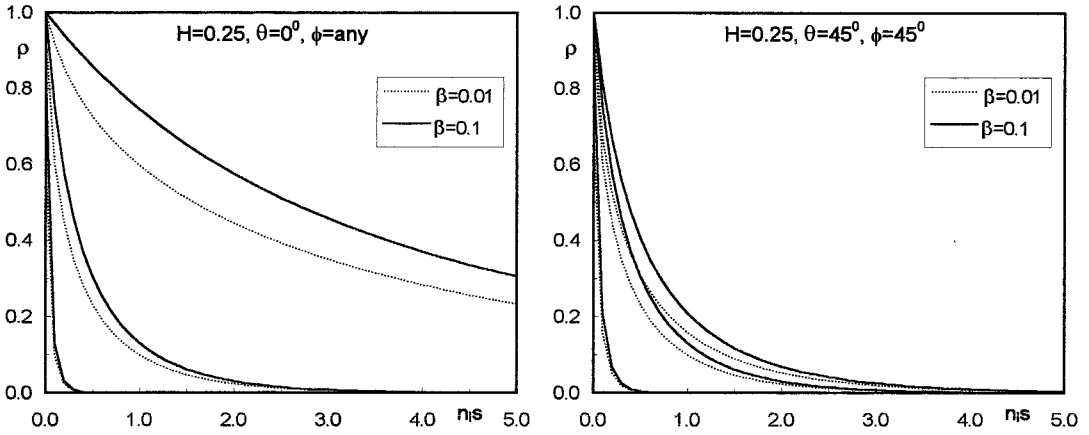

Figure 5. Autocorrelation function corresponding to anisotropic exponential modes with low- and high-frequency cutoffs versus dimensionless distance $n_l s$ for $H = 0.25$ and various e (from bottom to top, $e = 0.1$, 1, and 10), β, and angles θ and ϕ.

$$S(k^*, n_m) = \frac{2He_2e_3C_0}{\pi^2\Gamma(1-2H)(3+2H)n_m^{3+2H}} \cdot \mathrm{F}_{2,1}\left(2, \frac{3}{2}+H, \frac{5}{2}+H, -\frac{k^{*2}}{n_m^2}\right) \tag{38}$$

$$S(k^*, n_m) = \frac{2^{2H}HC_0'e_2e_3}{\pi^{3/2}\Gamma(1-H)k^{*(3+2H)/2}}\,\gamma'\left(\frac{3+2H}{2}, -\frac{n_m^2k^{*2}}{\pi}\right) \tag{39}$$

for superimposed exponential and Gaussian modes, respectively. Here $\mathrm{F}_{2,1}$ is the Gauss hypergeometric function, and $\gamma'(a, x) = \Gamma(a) - \Gamma(a, x)$ is the incomplete gamma function [*Abramowitz and Stegun*, 1972, p. 260, p. 556].

3. Lacunary Multiscale Random Field as a Weighted Superposition of Mutually Uncorrelated Modes

Lacunarity represents gaps in the multiscale hierarchy created by the absence of modes associated with discrete ranges of scales. Our theory allows us to account for such gaps in a straightforward manner by introducing intermediate cutoffs into the weighted superposition of exponential or Gaussian modes. For this purpose we designate M sets of lower and upper frequency cutoffs $n_{li} = 1/\lambda_{li}$ and $n_{ui} = 1/\lambda_{ui}$ ($i = 1, 2, \cdots, M$) such that $0 \le n_{ui} \le n_{l(i+1)}$ (Figure 6), define lacunae as all sets of modes corresponding to $n_{ui} < n < n_{l(i+1)}$, and construct our multiscale field as a weighted superposition of all remaining modes according to

$$\gamma(s^*, n_{l1}, n_{u1}, \cdots, n_{lM}, n_{uM}) = \sum_{i=1}^{M} \int_{n_{li}}^{n_{ui}} \gamma(s^*, n)\,\frac{dn}{n} \tag{40}$$

where s^* was defined in (8). Performing the integration yields

$$\gamma(s^*, n_{l1}, n_{u1}, \cdots, n_{lM}, n_{uM}) = \sum_{i=1}^{M} \gamma(s^*, n_{li}, n_{ui}) \tag{41}$$

where $\gamma(s^*, n_{li}, n_{ui})$ is given by (17). The variance, autocovariance, and integral scale of this lacunary multiscale field are given by

$$\sigma^2(n_{l1}, n_{u1}, \cdots, n_{lM}, n_{uM}) = \sum_{i=1}^{M} \sigma^2(n_{li}, n_{ui}) \tag{42}$$

$$C(s^*, n_{l1}, n_{u1}, \cdots, n_{lM}, n_{uM}) = \sum_{i=1}^{M} C(s^*, n_{li}, n_{ui}) \tag{43}$$

$$I(n_{l1}, n_{u1}, \cdots, n_{lM}, n_{uM}) = \frac{2H}{1+2H}\,\frac{\sum_{i=1}^{M}\left(\frac{1}{n_{li}^{1+2H}} - \frac{1}{n_{ui}^{1+2H}}\right)}{\sum_{i=1}^{M}\left(\frac{1}{n_{li}^{2H}} - \frac{1}{n_{ui}^{2H}}\right)}\,(\mathbf{u}^T\boldsymbol{\delta}^{-2}\mathbf{u})^{1/2} \tag{44}$$

respectively, where $\sigma^2(n_{li}, n_{ui})$ is defined in analogy to (20) and $C(s^*, n_{li}, n_{ui})$ is defined in analogy to (21) for any i. In the special case where $M = 1$, (44) reduces to (22). The term

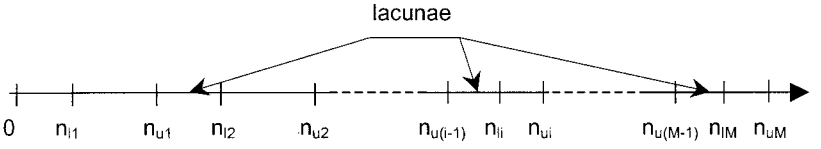

Figure 6. Discrete ranges of modes in multiscale hierarchy with lacunae $n_{ui} < n < n_{l(i+1)}$ along n axis.

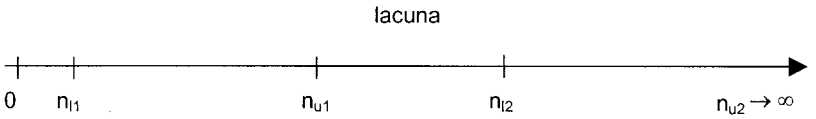

Figure 7. Two discrete ranges of modes in multiscale hierarchy with one lacuna $n_{u1} < n < n_{l2}$ when $n_{u2} \to \infty$.

raised to power ½ in (44) becomes unity when the multiscale field is isotropic.

To illustrate the properties of lacunary fields, we consider the simple case of a single gap, or lacuna, separating two sets of modes ($M = 2$) with $n_{u2} \to \infty$ as depicted in Figure 7. Our results below are given in terms of two dimensionless parameters, $\beta_1 = n_{l1}/n_{u1}$ and $c = (n_{l2} - n_{u1})/n_{l1}$. When $\beta_1 = 1$, the leftmost set of lower-frequency modes disappears; as β_1 decreases, the range of frequencies occupied by this set increases; when $\beta_1 = 0$, the leftmost set covers all frequencies from the lowest cutoff to infinity. The parameter c measures the length of the gap relative to the lowest cutoff; when there is no gap, $c = 0$. Figure 8 shows how the variance of such a lacunary field, normalized with respect to its lacuna-free value corresponding to $c = 0$, varies with β_1 for various values of H and c. For given H and c the variance decreases monotonically as β_1 increases. This is easily understood by fixing n_{l1} so that the process represents a gap of constant length in Figure 7, moving to the left along the n axis into the domain of lower frequencies which, by virtue of (5), are associated with larger variances (which, when cut out, reduce the overall variance of the multiscale hierarchy). For given H and β_1 the variance decreases as c increases, which is understood upon fixing both n_{l1} and n_{u1} so that the process represents a lacuna with fixed low-frequency edge, which widens by cutting out more and more high-frequency modes thereby reducing the overall variance. Figure 9 shows how the integral scale of the same lacunary field, normalized with respect to its lacuna-free value corresponding to $c = 0$, varies with β_1 for various values of H and c when all modes are isotropic. For given H and c the integral scale first increases with β_1 and then decreases. For a fixed nonzero n_{l1}, $\beta_1 = 0$ corresponds to an infinite high-frequency cutoff, n_{u1}. A corresponding increase in β_1 represents a decreasing high-frequency cutoff and a corresponding elimination of small-scale contributions to the integral scale of the multiscale hierarchy, which therefore increases with β_1. As β_1 approaches 1, the leftmost set of lower-frequency modes (Figure 7) is gradually eliminated by the lacuna, so that small-

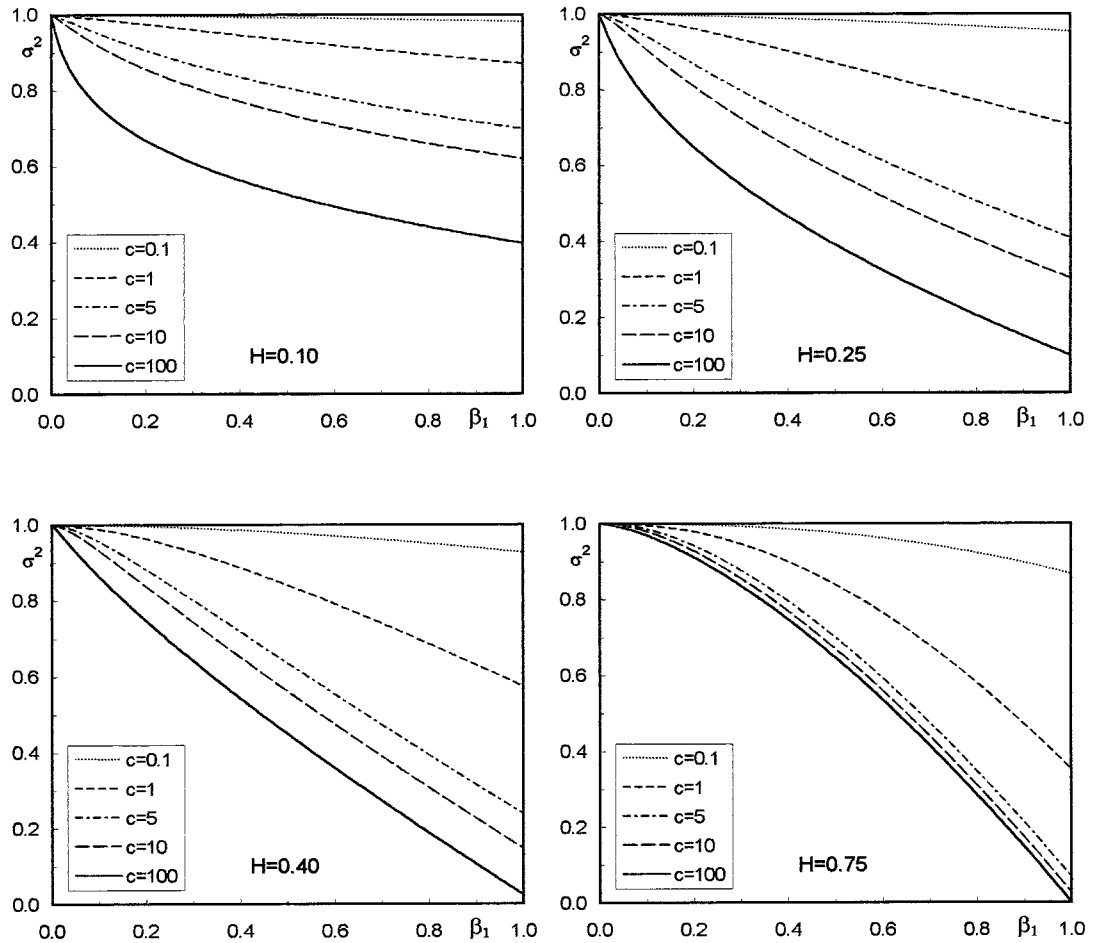

Figure 8. Dimensionless variance versus β_1 for various c and H corresponding to single lacuna.

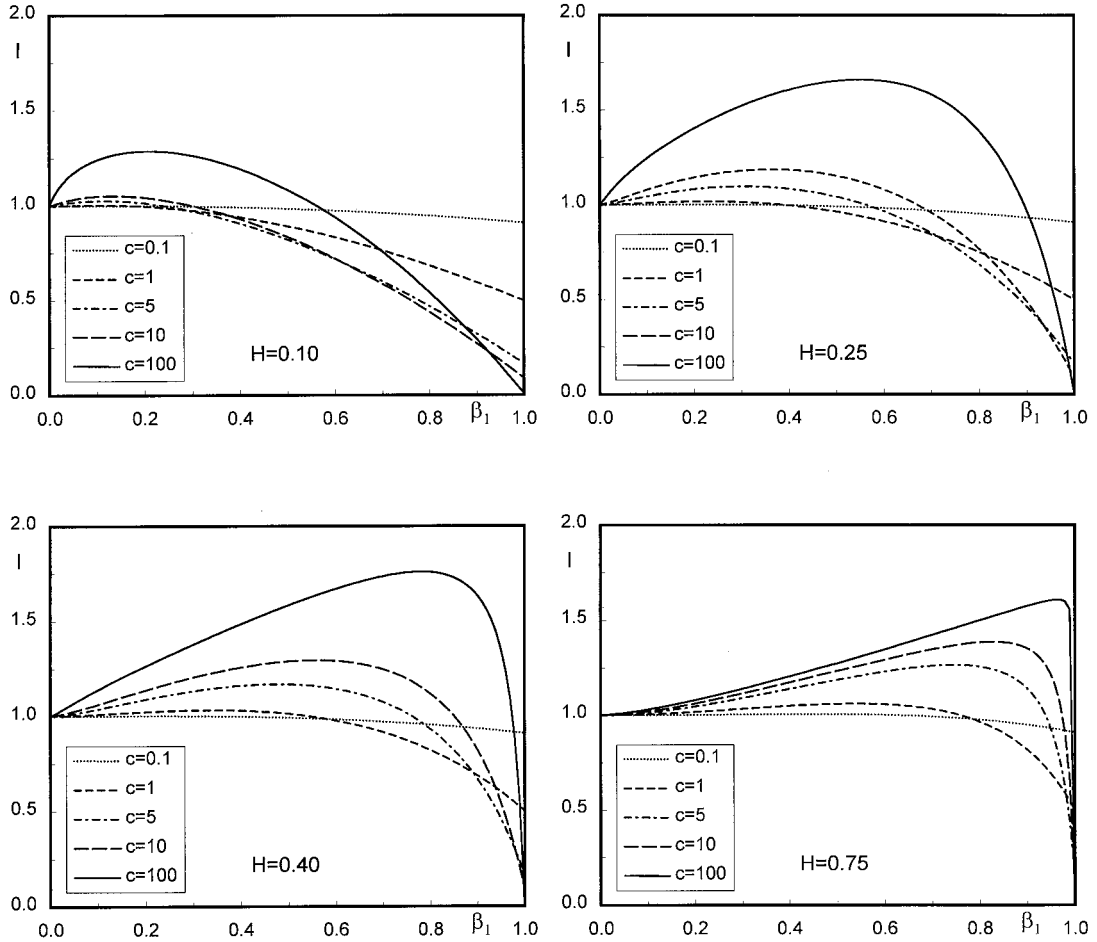

Figure 9. Dimensionless isotropic integral scale versus β_1 for various c and H corresponding to single lacuna.

scale contributions to the integral scale of the hierarchy become predominant and cause the latter to diminish. At relatively small values of β_1 the integral scale increases with c; as n_{l2} grows while n_{l1} and n_{u1} are fixed, the gap gradually extends into the rightmost set of high-frequency modes whose influence on the integral scale thereby diminishes, allowing the latter to increase. As β_1 approaches 1, the integral scale decreases with c as the leftmost set of low-frequency modes narrows down. The rates at which the variance and integral scale in Figures 8 and 9 vary with β_1 and c depend strongly on H.

Figures 10 and 11 depict the autocorrelations $\rho(s, n_{l1}, n_{u1}, n_{l2}) = C(s, n_{l1}, n_{u1}, n_{l2})/\sigma^2(n_{l1}, n_{u1}, n_{l2})$ corresponding to isotropic exponential and Gaussian modes, respectively, as functions of dimensionless distance $n_l s$ for various values of H, β_1, and c. The autocorrelation generally increases with H and c except at values of β_1 close to 1 where it sometimes decreases as c increases. Autocorrelations corresponding to exponential modes exhibit longer tails than those corresponding to Gaussian modes.

We close this section by examining briefly the combined effects of anisotropy and lacunarity on the integral scale and autocorrelation of a multiscale random field. We do so for the special case of axisymmetric anisotropy ($e_2 = 1$, $e_3 = e$) at $H = 0.25$. Figure 12 shows how the integral scale, normalized with respect to its horizontal value corresponding to $\beta_1 = 0$ and $c = 0$, varies with the angle of inclination θ from the vertical for various values of β_1, c, and the axisymmetric anisotropy ratio e which takes on, from bottom to top, the values 0.01, 0.1, 1, 10, and 100. When $e < 1$ so that the spatial autocorrelation scales of each mode are larger in the horizontal than in the vertical direction, the normalized integral scale of the truncated hierarchy increases with θ; it decreases with θ when $e > 1$. In the isotropic case where $e = 1$, the normalized integral scale of the hierarchy does not vary with θ. In all cases it decreases slightly with β_1 and is relatively insensitive to c.

Autocorrelation functions $\rho(s, n_{l1}, n_{u1}, n_{l2}, e) = C(s, n_{l1}, n_{u1}, n_{l2}, e)/\sigma^2(n_{l1}, n_{u1}, n_{l2})$ along the vertical ($\theta = 0°$, any ϕ) and an inclined ($\theta = 45°$, $\phi = 45°$) direction corresponding to exponential modes, $H = 0.25$, two values of β_1 and c each, and three values of e (equal to 0.1, 1, and 10 from bottom to top) are plotted versus $n_l s$ in Figure 13. Their decay rate is seen to increase with β_1, c, and inclination from the vertical.

4. Upscaled Conductivity and Its Autocovariance

Tartakovsky and Neuman [1998] have recently developed analytical expressions for effective hydraulic conductivity under three-dimensional transient flow through a box-shaped domain because of a mean hydraulic gradient that varies slowly in space and time. Their box is embedded within a statistically homogeneous natural log hydraulic conductivity field, $Y(\mathbf{x})$, that is Gaussian and exhibits an anisotropic spatial correlation

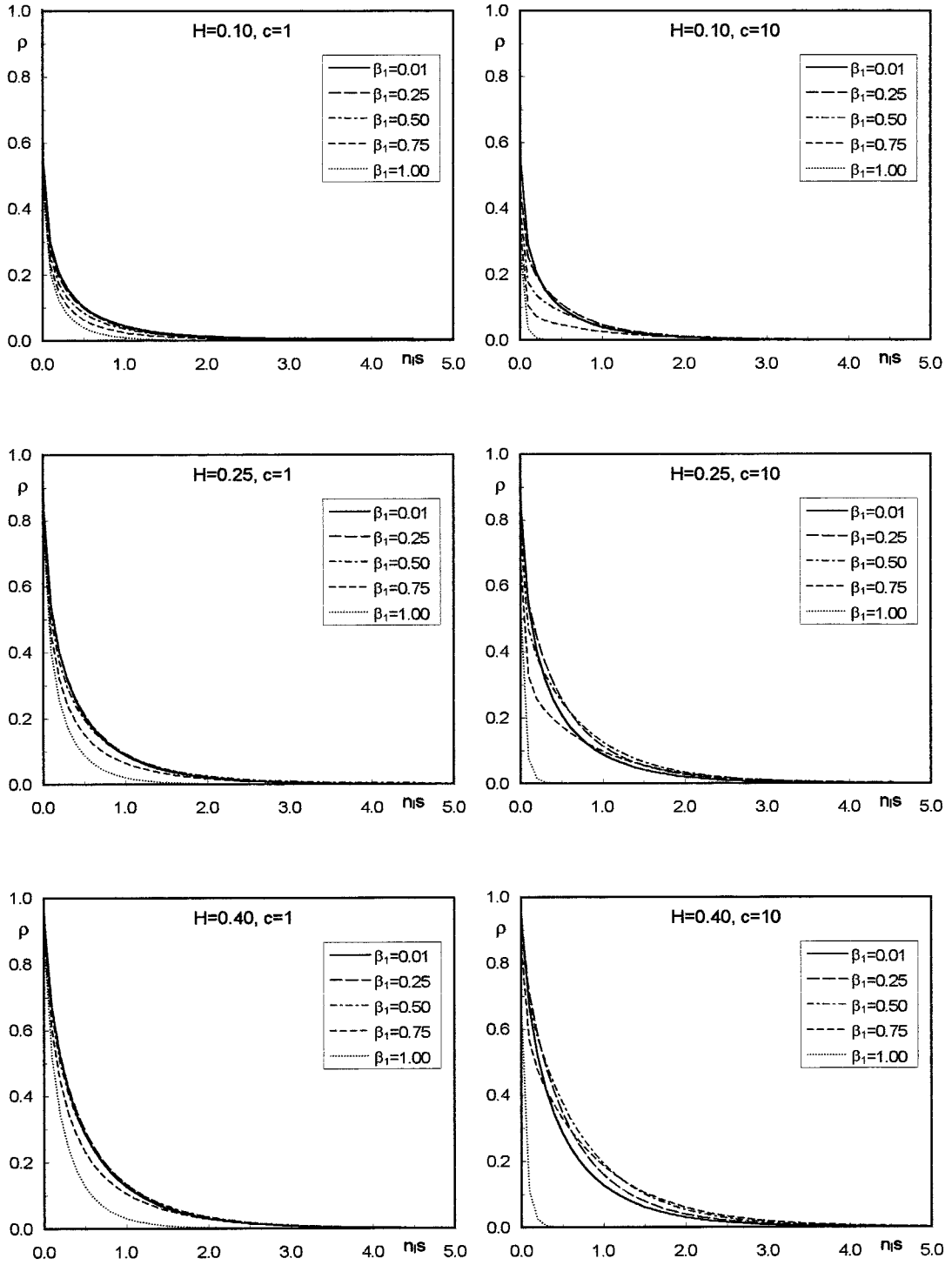

Figure 10. Isotropic autocorrelation function corresponding to exponential modes with single lacuna versus dimensionless distance $n_l s$ for various β_1, c, and H.

structure. Here we consider their steady state result for a box with lateral mean no-flow boundaries separated by finite distances equal to L_2 and L_3 and two constant head boundaries a distance L_1 apart (Figure 14). The boundaries of the box are parallel to the principal coordinates of statistical anisotropy. A spatially uniform mean hydraulic gradient $\mathbf{J}$ of magnitude J_1 acts between the Dirichlet boundaries parallel to x_1. Then, according to (29) of *Tartakovsky and Neuman* [1998],

$$\frac{K_{\text{eff}}^{[2]}(\mathbf{x})}{K_G} = 1 + \sigma_Y^2[\tfrac{1}{2} - D_{st}(\mathbf{x})] \tag{45}$$

where $K_{\text{eff}}^{[2]}$ is the principal effective hydraulic conductivity parallel to x_1, valid to first order of approximation in the variance σ_Y^2 of Y (or to second order in σ_Y, as implied by the bracketed superscript), K_G is the geometric mean of hydraulic conductivity K, D_{st} is given by their (22) as

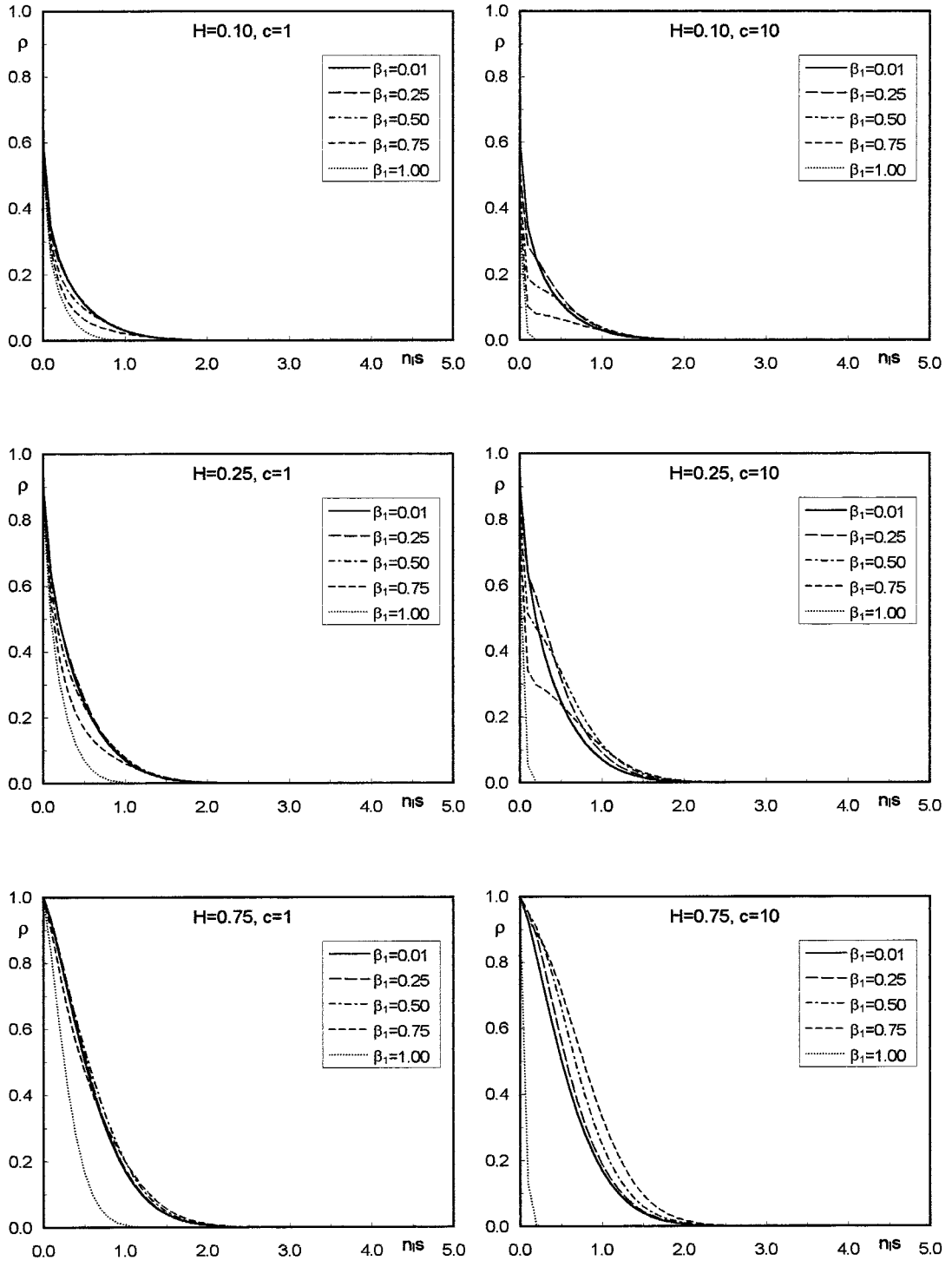

Figure 11. Same as Figure 10 but corresponding to Gaussian modes.

$$D_{st}(\mathbf{x}) = \int_0^{L_1}\int_0^{L_2}\int_0^{L_3} \rho_Y(\mathbf{x}, \mathbf{y})\, \frac{\partial^2 G_K(\mathbf{x}, \mathbf{y})}{\partial x_1 \partial y_1}\, d\mathbf{y} \qquad (46)$$

where ρ_Y is the spatial autocorrelation function of Y, and G_K is a Green's function defined as the solution of $\nabla^2 G_K(\mathbf{x}, \mathbf{y}) = 0$ in the box (Appendix B). A conjecture due to *Landau and Lifschitz* [1960] allows generalizing (45) to arbitrary σ_Y^2 by writing

$$\frac{K_{\text{eff}}(\mathbf{x})}{K_G} = \exp\{\sigma_Y^2[\tfrac{1}{2} - D_{st}(\mathbf{x})]\} \qquad (47)$$

In the paper of *Tartakovsky and Neuman* [1998], ρ_Y corresponds to a single exponential mode of our truncated multiscale hierarchy. In this paper we set ρ_Y in (46) equal to

$$\rho_Y(s^*, \lambda_l) = \exp\left(-\frac{s^*}{\lambda_l}\right) - \left(\frac{s^*}{\lambda_l}\right)^{2H} \Gamma\left(1 - 2H, \frac{s^*}{\lambda_l}\right) \qquad (48)$$

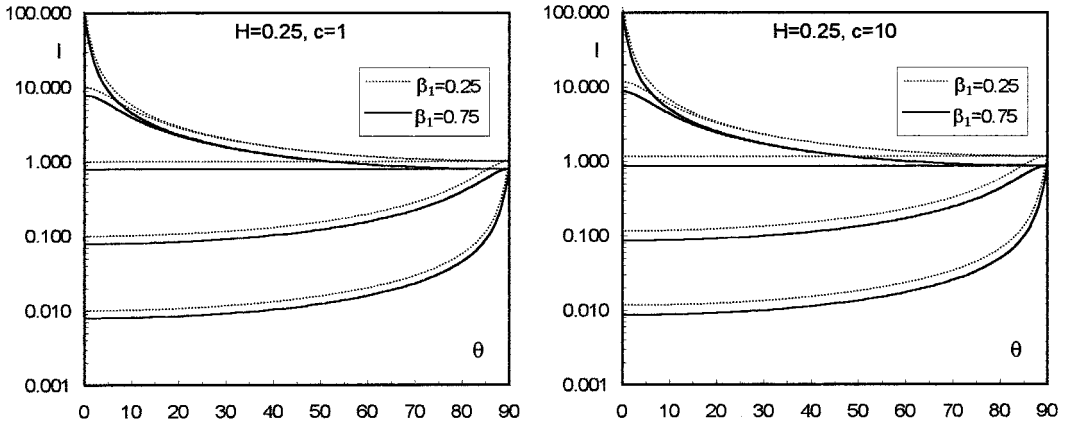

Figure 12. Dimensionless integral scale versus angle θ for various e (from bottom to top, $e = 0.01$, 0.1, 1, 10, and 100), β_1, and c corresponding to single lacuna when $H = 0.25$.

which is obtained upon substituting (19) into (21) and taking $n_u \to \infty$. The latter corresponds to a multiscale hierarchy of exponential modes with a low-frequency cutoff scale (in the principal x_1 direction) λ_l, and anisotropy ratios $e_i = I_i/I_1$, expressed in terms of a scalar separation distance $s^* = |\mathbf{x}^* - \mathbf{y}^*|$ defined in equivalent isotropic coordinates $x_i^* = x_i/e_i$. In accord with *Di Federico and Neuman* [1997] we set $\lambda_l = \mu L_1$ so that $x_i^*/\lambda_l = x_i^*/(\mu L_1) = x_i/(\mu e_i L_1) = \chi_i/\mu$, where $\chi_i = x_i/L_i$, which allows us to rewrite (48) as

$$\rho_Y(r, \mu) = \exp\left(-\frac{r}{\mu}\right) - \left(\frac{r}{\mu}\right)^{2H} \Gamma\left(1 - 2H, \frac{r}{\mu}\right) \qquad (49)$$

$$r = |\boldsymbol{\chi} - \boldsymbol{\zeta}|$$

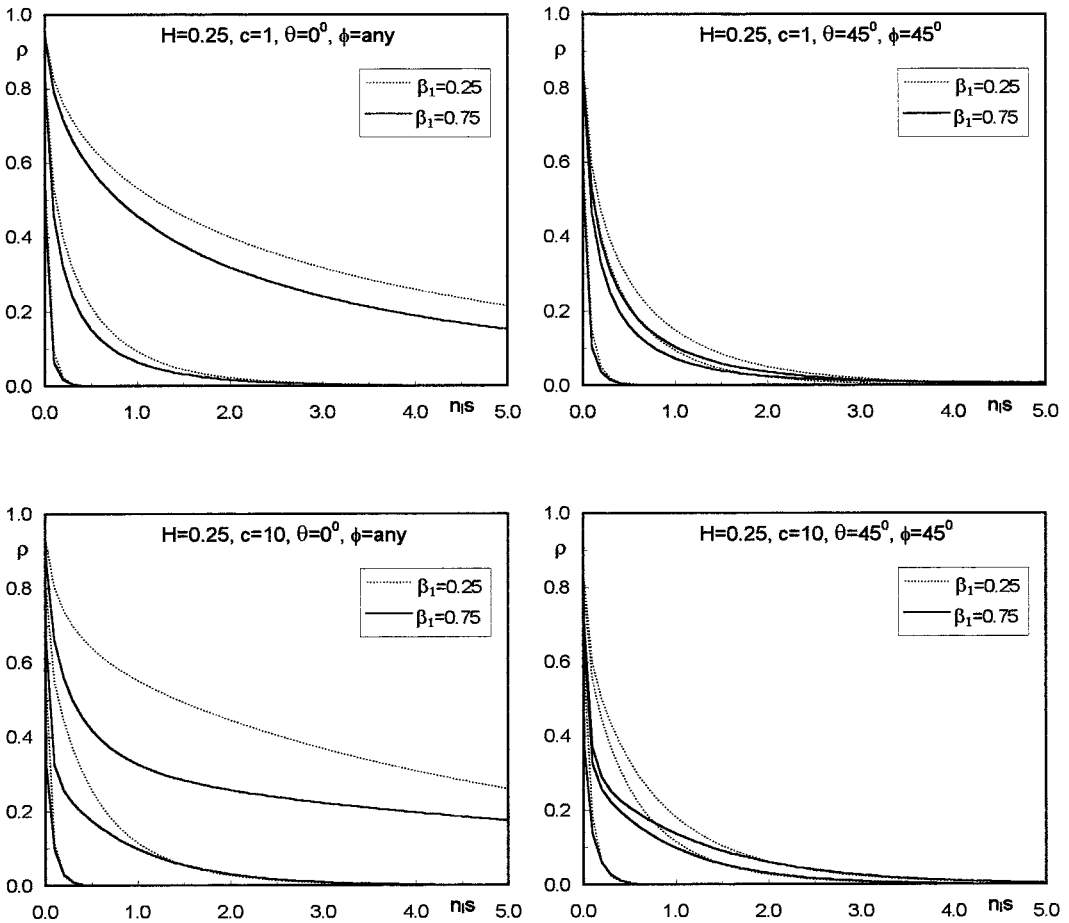

Figure 13. Autocorrelation function corresponding to anisotropic exponential modes with single lacuna versus dimensionless distance $n_l s$ for various e (from bottom to top, $e = 0.1$, 1, and 10), β_1, c, and angles θ, ϕ when $H = 0.25$.

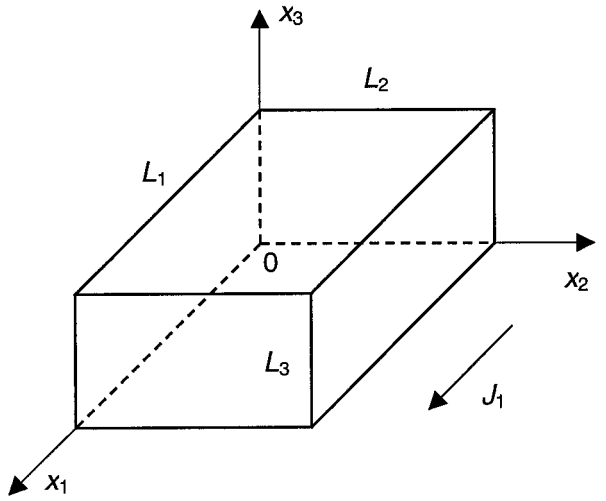

Figure 14. Box-shaped flow domain with Dirichlet and Neumann boundaries.

As shown in Appendix A, (46) then takes the form

$$D_{st}(\boldsymbol{\chi}) = \frac{e_2 e_3}{8\pi^{3/2}} \int_0^\infty \int_0^1 \int_0^1 \int_0^1 \eta^{-5/2} \rho_Y(r, \mu) \sum_{m=-\infty}^{\infty} \left[\left(\frac{1}{2} - \frac{a_m^+}{\eta} \right) \cdot \exp\left(-\frac{a_m^+}{\eta} \right) + \left(\frac{1}{2} - \frac{a_m^-}{\eta} \right) \exp\left(-\frac{a_m^-}{\eta} \right) \right] \cdot \sum_{n=-\infty}^{\infty} \left[\exp\left(-\frac{b_n^+}{\eta} \right) + \exp\left(-\frac{b_n^-}{\eta} \right) \right] \cdot \sum_{j=-\infty}^{\infty} \left[\exp\left(-\frac{c_j^+}{\eta} \right) + \exp\left(-\frac{c_j^-}{\eta} \right) \right] d\zeta_1\, d\zeta_2\, d\zeta_3\, d\eta \tag{50}$$

where $a_m^{\pm}$, $b_j^{\pm}$, and $c_j^{\pm}$ are defined in (B11). On the basis of their Figure 9, *Di Federico and Neuman* [1997] found that the integral scale of a truncated multiscale hierarchy is of the order of one tenth the length of a corresponding sampling window. If we consider our box to represent such a window, then their finding implies that $I_i \approx L_i/10$. The latter, coupled with (50) and (51) of Di Federico and Neuman, implies that

$$\frac{2H}{1+2H}\,\mu \approx \frac{1}{10} \tag{51}$$

where, for exponential modes, $0 < H < 1/2$. It thus follows that D_{st} is a function of H and anisotropy ratios but not of either box size or σ_Y^2. However, K_{eff} increases linearly (in the case of (45)) or exponentially (in the case of (47)) with σ_Y^2, which, in turn, is proportional to $\lambda_I^{2H} = (\mu L_1)^{2H}$ and thereby renders K_{eff} a function of box size.

As $D_{st}(\boldsymbol{\chi})$ is formally a function of $\boldsymbol{\chi}$, we evaluate it at the midpoint $\boldsymbol{\chi} = (0.5, 0.5, 0.5)$ of the box. Figure 15 shows how D_{st} at this point, normalized by the product $e_2 e_3$, varies with H when the latter is related to μ according to (51). It is seen that D_{st} increases monotonically with the Hurst coefficient within its admissible range, $0 < H < 0.5$, rapidly at small values of H and more slowly at higher values. The corresponding variation of K_{eff}/K_G with L_1, according to (47), is depicted for selected values of H in Figure 16. As implied by (47), K_{eff}/K_G increases exponentially (and its logarithm linearly) with L_1^{2H}, in agreement with an earlier expression proposed by *Neuman* [1994] for a block of length scale L without accounting for truncation. Our (47) is identical to (4) of Neuman provided one interprets his variogram as our σ_Y^2 and sets his boundary factor β (in our three-dimensional case) equal to $3D_{st}$.

In deriving the above expressions for K_{eff} in a box of dimensions L_1, L_2, and L_3, we excluded (filtered out) all modes having integral scales larger than $\lambda_{Ii} = \mu L_i (i = 1, 2, 3)$. The unfiltered modes form a homogeneous field with well-defined variance σ_Y^2, autocorrelation function ρ_Y, and principal integral scales I_i. These quantities represent measures of how the unfiltered, small-scale or high-frequency modes fluctuate about a mean, $\langle Y \rangle$, which the filtering process leaves undefined. This is so because $\langle Y \rangle$ is determined by the large-scale, low-frequency modes that have been filtered out. It follows that our expressions for K_{eff} are conditional on a knowledge of $\langle Y \rangle = \ln K_G$ within the box.

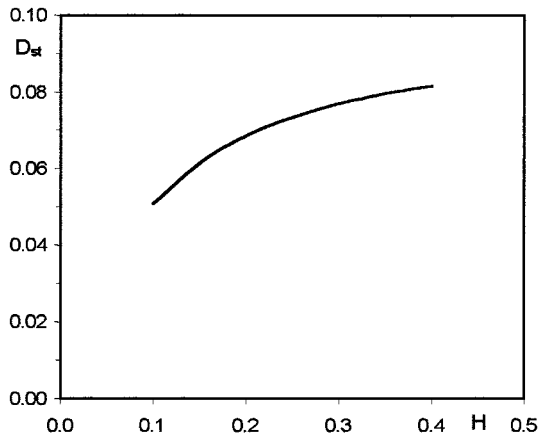

Figure 15. D_{st} normalized by $e_2 e_3$ versus H.

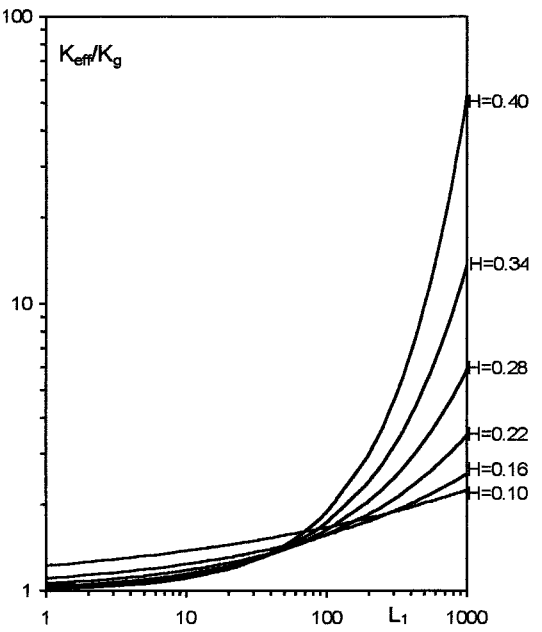

Figure 16. K_{eff}/K_G versus L_1 for various H.

Taking the natural logarithm of (47) yields

$$Y_{\text{eff}} = \langle Y \rangle + \sigma_Y^2(\tfrac{1}{2} - D_{st}) \tag{52}$$

where $Y_{\text{eff}} = \ln K_{\text{eff}}$ and the rightmost term is independent of $\langle Y \rangle$. It follows that any uncertainty in $\langle Y \rangle$ translates directly into an identical uncertainty in Y_{eff}. To quantify this uncertainty, we embed the box in a larger domain of dimensions B_1, B_2, and B_3 such that $B_i \geq L_i$ for all i (Figure 17). It is convenient (though not necessary) to think of the larger domain as a flow region, to think of the box as an element of a computational grid superimposed on this region, and to think of K_{eff} as an upscaled or equivalent conductivity assigned to this element. Then (52) implies that Y_{eff} consists of two additive components, $\langle Y \rangle$ which accounts for fluctuations in Y on scales larger than a grid block and can therefore be resolved by the grid and $\sigma_Y^2(1/2 - D_{st})$ which accounts for unresolved subgrid fluctuations.

Let $\tilde{\lambda}_{Ii} = \mu B_i$ be principal integral cutoff scales associated with the flow domain. Then the modes that contribute to fluctuations in $\langle Y \rangle$ within the flow domain have principal integral scales $\lambda_{Ii} \leq \lambda_i \leq \tilde{\lambda}_{Ii}$. It follows immediately that the superimposed hierarchy of these modes has a variance

$$\sigma_Y^2(\tilde{n}_I, n_I) = \sigma_Y^2(\tilde{n}_I) - \sigma_Y^2(n_I) \tag{53}$$

and autocorrelation function

$$\rho_Y(s^*, \tilde{n}_I, n_I) = \rho_Y(s^*, \tilde{n}_I) - \rho_Y(s^*, n_I) \tag{54}$$

where $\tilde{n}_I = 1/\tilde{\lambda}_{I1}$, $\sigma_Y^2(n_I) = \sigma_Y^2$ is the variance of the subgrid fluctuations, and $\rho_Y(s^*, n_I)$ is their autocorrelation function. Clearly, (53) and (54) represent the variance and autocorrelation of $\langle Y \rangle$ and therefore Y_{eff}, within the flow domain.

5. Conclusions

The following conclusions can be drawn from this paper:

1. Both the power (semi)variogram and associated spectra of a random field with homogeneous anisotropic increments can be constructed mathematically as (decomposed into) weighted integrals from zero to infinity (an infinite hierarchy) of either exponential or Gaussian variograms and spectra of uncorrelated homogeneous, statistically anisotropic random fields (modes) with identical anisotropy ratios. Regardless of how one constructs (or decomposes) the hierarchical field, the latter is nonhomogeneous, positively autocorrelated across all scales, and constitutes an anisotropic random fractal. This result is valid for exponential modes when the Hurst coefficients is in the range $0 < H < \frac{1}{2}$ and for Gaussian modes when it is in the range $0 < H < 1$.

2. We investigated mathematically the effect of filtering out (truncating) high- and low-frequency (small and large scale) modes from this infinite hierarchy in three-dimensional real and spectral domains. A low-frequency cutoff renders the truncated hierarchy statistically homogeneous with a positive spatial autocovariance function that decays monotonically with separation distance. The principal integral scales of the lowest-frequency mode (cutoff) are related to corresponding length scales of a sampling window defined by the domain under investigation. The principal integral scale of the highest-frequency mode (cutoff) is related to corresponding length scales of the data support (volume of measurement). Taking each relationship to be one of proportionality renders our expressions for the variance and principal integral scales of a truncated anisotropic multiscale field explicitly dependent on characteristic length scales of the sampling window and data support.

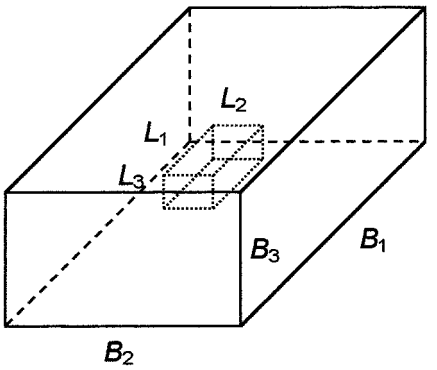

Figure 17. Box-shaped domain (block) embedded into larger domain (flow region).

3. When the characteristic length scale of the sampling window is much larger than that of the data support, the variance of the truncated hierarchy increases as a power $2H$ of this characteristic scale, and the principal integral scales increase linearly with the same scale.

4. Our theory allows accounting for lacunarity due to gaps in the multiscale hierarchy, created by the absence of modes associated with discrete ranges of scales, through the introduction of intermediate cutoffs. We have shown that the variance, autocorrelation function, and principal integral scales of an anisotropic multiscale field with a single lacuna depend on its range of modes relative to the lower and upper cutoff modes of the field.

5. We developed expressions for the principal effective hydraulic conductivity K_{eff} of a box-shaped porous block, embedded within a three-dimensional anisotropic multiscale log hydraulic conductivity field, under mean-uniform steady state flow parallel to a principal direction of anistropy. We did so for a block that is much larger than the support scale of the field, which can therefore be set equal to zero; however, a nonzero support is easy to accommodate. The effective conductivity was shown to depend on the Hurst coefficient H, anisotropy ratios, and a characteristic length scale of the box raised to power $2H$. It was additionally shown to be conditional on knowledge of mean log conductivity within the box.

6. The mean log conductivity within the box is a random variable which depends on low-frequency modes that had been excluded (filtered out) from our evaluation of the effective conductivity K_{eff}. Our theory allows quantifying the variance and spatial autocorrelation of this random variable, as well as those of its natural logarithm, $Y_{\text{eff}} = \ln K_{\text{eff}}$, by embedding the box in a larger domain. It is convenient (though not necessary) to think of this larger domain as a flow region, to think of the box as an element of a computational grid superimposed on this region, and to think of K_{eff} as an upscaled or equivalent conductivity assigned to this element. Then our theory allows representing Y_{eff} as the sum of two well-defined components, one which accounts for fluctuations in log conductivity on scales larger than a grid block and can therefore be resolved by the grid and another which accounts for unresolved subgrid fluctuations.

7. Our theory includes new expressions for the anisotropic

variograms of multiscale random functions, with continuous or discontinuous (lacunary) ranges of scale, which can be used to perform standard geostatistical analyses of such functions, including kriging, cokriging, and conditional simulation. All that is required to make this computationally feasible is to embed our new variogram expressions in existing or newly developed geostatistical software. The same expressions make it possible to apply standard methods of unconditional and conditional stochastic analysis, such as perturbation, to flow and transport in anisotropic, lacunary multiscale fields of heterogeneity. All that is required for this purpose is to replace the single-scale covariance functions, which are used to represent medium heterogeneity in existing stochastic theories and models, with the multiscale functions we present in this paper.

Appendix A: Derivation of D_{st}

As $e_1 = 1$, it follows that

$$\frac{\partial^2}{\partial x_1 \partial y_1} = \frac{\partial^2}{\partial x_1^* \partial y_1^*} \tag{A1}$$

The cross derivative of the Green function $G_K(\mathbf{x}^*, \mathbf{y}^*)$ in (46) is given by (B13). Combining (46), (48), and (B13) leads to

$$D_{st}(\mathbf{x}^*) = \frac{1}{8\pi^{3/2} L_1^* L_2^* L_3^*} \int_0^\infty \int_0^{L_1} \int_0^{L_2} \int_0^{L_3} \eta^{-5/2} \rho_Y(s^*, \lambda_l)$$

$$\cdot \sum_{m=-\infty}^{\infty} \left[\left(\frac{1}{2} - \frac{a_m^+}{\eta} \right) \exp\left(-\frac{a_m^+}{\eta} \right) + \left(\frac{1}{2} - \frac{a_m^-}{\eta} \right) \exp\left(-\frac{a_m^-}{\eta} \right) \right]$$

$$\cdot \sum_{n=-\infty}^{\infty} \left[\exp\left(-\frac{b_n^+}{\eta} \right) + \exp\left(-\frac{b_n^-}{\eta} \right) \right]$$

$$\cdot \sum_{j=-\infty}^{\infty} \left[\exp\left(-\frac{c_j^+}{\eta} \right) + \exp\left(-\frac{c_j^-}{\eta} \right) \right] d\mathbf{y}\, d\eta \tag{A2}$$

where the coefficients $a_m^{\pm}$, $b_n^{\pm}$, $c_n^{\pm}$ are defined in (B11). Upon introducing a new variable of integration

$$\zeta_i = y_i / L_i \tag{A3}$$

while considering (49), (A2) leads directly to (50).

Appendix B: Derivation of the Green's Function

To the best of our knowledge the Green's function $G(\mathbf{x}, \mathbf{y})$ for the three-dimensional Laplace equation in the box considered in the paper is not given in the literature. At the same time the Green's function $G_D(\mathbf{x}, \mathbf{y}, t - \tau)$ for the diffusion equation has the form [*Tartakovsky*, 1996, equation (3.57)]

$$G_D(\mathbf{x}^*, \mathbf{y}^*, \eta) = \frac{2}{L_1^* L_2^* L_3^*} \sum_{m=1}^{\infty} \exp\left(-\frac{D\pi^2 \eta m^2}{L_1^{*2}} \right)$$

$$\cdot \sin\left(\frac{\pi m x_1^*}{L_1^*} \right) \sin\left(\frac{\pi m y_1^*}{L_1^*} \right)$$

$$\cdot \left[1 + 2 \sum_{n=1}^{\infty} \exp\left(-\frac{D\pi^2 \eta n^2}{L_2^{*2}} \right) \cos\left(\frac{\pi n x_2^*}{L_2^*} \right) \cos\left(\frac{\pi n y_2^*}{L_2^*} \right) \right]$$

$$\cdot \left[1 + 2 \sum_{j=1}^{\infty} \exp\left(-\frac{D\pi^2 \eta j^2}{L_3^{*2}} \right) \cos\left(\frac{\pi j x_3^*}{L_3^*} \right) \cos\left(\frac{\pi j y_3^*}{L_3^*} \right) \right] \tag{B1}$$

where $D = K_G/S$ is the diffusion coefficient, and $\eta = t - \tau$. We require the derivative

$$\frac{\partial^2 G_D(\mathbf{x}^*, \mathbf{y}^*, \eta)}{\partial x_1^* \partial y_1^*} = \frac{2\pi^2}{L_1^{*3} L_2^* L_3^*} \sum_{m=1}^{\infty} m^2 \exp\left(-\frac{D\pi^2 \eta m^2}{L_1^{*2}} \right)$$

$$\cdot \cos\left(\frac{\pi m x_1^*}{L_1^*} \right) \cos\left(\frac{\pi m y_1^*}{L_1^*} \right)$$

$$\cdot \left[1 + 2 \sum_{n=1}^{\infty} \exp\left(-\frac{D\pi^2 \eta n^2}{L_2^{*2}} \right) \cos\left(\frac{\pi n x_2^*}{L_2^*} \right) \cos\left(\frac{\pi n y_2^*}{L_2^*} \right) \right]$$

$$\cdot \left[1 + 2 \sum_{j=1}^{\infty} \exp\left(-\frac{D\pi^2 \eta j^2}{L_3^{*2}} \right) \cos\left(\frac{\pi j x_3^*}{L_3^*} \right) \cos\left(\frac{\pi j y_3^*}{L_3^*} \right) \right] \tag{B2}$$

Owing to slow rate of convergence of (B1) it is advantageous to work with an alternative representation of G_D, obtained by means of Poisson's summation formula [*Tartakovsky*, 1996, Appendix I]. Before applying the latter, we introduce the dimensionless variables

$$t_D = \frac{Dt}{L_1^2} \qquad \hat{x}_i = \frac{x_i^*}{L_1} \tag{B3}$$

Upon recalling that $e_i = I_i/I_1$ and $x_i^* = x_i/e_i$, one has

$$\frac{Dt}{L_i^{*2}} = \frac{Dte_i^2}{L_i^2} = \frac{L_1^2 e_i^2}{L_i^2} t_D = \frac{L_1^2 I_i^2}{I_1^2 L_i^2} t_D = t_D \tag{B4}$$

$$\frac{x_i^*}{L_i^*} = \frac{L_1 x_i^*}{L_1^* L_1} = \frac{L_1 e_i}{L_i^2} \hat{x}_i = \frac{L_1 I_i}{I_1 L_i} \hat{x}_i = \hat{x}_i \tag{B5}$$

where, as discussed in the context of (51), we have set $L_i/I_i = 10$ for all i. Then (B2) becomes

$$\frac{\partial^2 G_D(\mathbf{x}^*, \mathbf{y}^*, \eta)}{\partial x_1^* \partial y_1^*}$$

$$= \frac{2\pi^2}{L_1^{*3} L_2^* L_3^*} \sum_{m=1}^{\infty} m^2 \exp\left(-\pi^2 \eta_D m^2 \right) \cos\left(\pi m \hat{x}_1 \right) \cos\left(\pi m \hat{y}_1 \right)$$

$$\cdot \left[1 + 2 \sum_{n=1}^{\infty} \exp\left(-\pi^2 \eta_D n^2 \right) \cos\left(\pi n \hat{x}_2 \right) \cos\left(\pi n \hat{y}_2 \right) \right]$$

$$\cdot \left[1 + 2 \sum_{j=1}^{\infty} \exp\left(-\pi^2 \eta_D j^2 \right) \cos\left(\pi j \hat{x}_3 \right) \cos\left(\pi j \hat{y}_3 \right) \right] \tag{B6}$$

It then follows from *Tartakovsky* [1996, equations (I5), (I10), (I11)] that

$$\sum_{m=1}^{\infty} m^2 \exp(-\pi^2\eta_D m^2)\cos(\pi m\hat{x}_1)\cos(\pi m\hat{y}_1)$$

$$= \frac{1}{16(\pi\eta_D)^{5/2}} \sum_{m=-\infty}^{\infty} \left\{ [2\eta_D - (\hat{x}_1 + \hat{y}_1 + 2m)^2] \cdot \exp\left[-\frac{(\hat{x}_1 + \hat{y}_1 + 2m)^2}{4\eta_D} \right] + [2\eta_D - (\hat{x}_1 - \hat{y}_1 + 2m)^2] \cdot \exp\left[-\frac{(\hat{x}_1 - \hat{y}_1 + 2m)^2}{4\eta_D} \right] \right\} \quad \text{(B7)}$$

$$\sum_{n=1}^{\infty} n^2 \exp(-\pi^2\eta_D n^2)\cos(\pi n\hat{x}_2)\cos(\pi n\hat{y}_2)$$

$$= -\frac{1}{2} + \frac{1}{4\sqrt{\pi\eta_D}} \sum_{n=-\infty}^{\infty} \left\{ \exp\left[-\frac{(\hat{x}_2 + \hat{y}_2 + 2n)^2}{4\eta_D} \right] + \exp\left[-\frac{(\hat{x}_2 - \hat{y}_2 + 2n)^2}{4\eta_D} \right] \right\} \quad \text{(B8)}$$

$$\sum_{j=1}^{\infty} j^2 \exp(-\pi^2\eta_D j^2)\cos(\pi j\hat{x}_3)\cos(\pi j\hat{y}_2)$$

$$= -\frac{1}{2} + \frac{1}{4\sqrt{\pi\eta_D}} \sum_{j=-\infty}^{\infty} \left\{ \exp\left[-\frac{(\hat{x}_3 + \hat{y}_3 + 2j)^2}{4\eta_D} \right] + \exp\left[-\frac{(\hat{x}_3 - \hat{y}_3 + 2j)^2}{4\eta_D} \right] \right\} \quad \text{(B9)}$$

Substituting (B7)–(B9) into (B6) yields

$$\frac{\partial^2 G_D(\mathbf{x}^*, \mathbf{y}^*, \eta_D)}{\partial x_1^* \partial y_1^*} = \frac{\eta_D^{-5/2}}{8\pi^{3/2} L_1^{*3} L_2^* L_3^*} \cdot \sum_{m=-\infty}^{\infty} \left[\left(\frac{1}{2} - \frac{a_m^+}{\eta_D} \right) \exp\left(-\frac{a_m^+}{\eta_D} \right) + \left(\frac{1}{2} - \frac{a_m^-}{\eta_D} \right) \exp\left(-\frac{a_m^-}{\eta_D} \right) \right] \cdot \sum_{n=-\infty}^{\infty} \left[\exp\left(-\frac{b_n^+}{\eta_D} \right) + \exp\left(-\frac{b_n^-}{\eta_D} \right) \right] \cdot \sum_{j=-\infty}^{\infty} \left[\exp\left(-\frac{c_j^+}{\eta_D} \right) + \exp\left(-\frac{c_j^-}{\eta_D} \right) \right] \quad \text{(B10)}$$

where

$$a_m^+ = \frac{(\hat{x}_1 + \hat{y}_1 + 2m)^2}{4} \quad a_m^- = \frac{(\hat{x}_1 - \hat{y}_1 + 2m)^2}{4}$$

$$b_n^+ = \frac{(\hat{x}_2 + \hat{y}_2 + 2n)^2}{4} \quad b_n^- = \frac{(\hat{x}_2 - \hat{y}_2 + 2n)^2}{4} \quad \text{(B11)}$$

$$c_j^+ = \frac{(\hat{x}_3 + \hat{y}_3 + 2j)^2}{4} \quad c_j^- = \frac{(\hat{x}_3 - \hat{y}_3 + 2j)^2}{4}$$

The Green's function G_K for the Laplace equation can be obtained from the corresponding Green's function G_D for the diffusion equation through the following relation

$$G_K(\mathbf{x}, \mathbf{y}) = \lim_{t_D \to \infty} \int_0^{t_D} G_D(\mathbf{x}, \mathbf{y}, \eta_D)\, d\eta_D \quad \text{(B12)}$$

where t_D is dimensionless time defined earlier. It thus follows from (B10) that

$$\frac{\partial^2 G_K(\mathbf{x}^*, \mathbf{y}^*)}{\partial x_1^* \partial y_1^*} = \frac{1}{8\pi^{3/2} L_1^{*3} L_2^* L_3^*} \cdot \int_0^{t_D} \eta_D^{-5/2} \sum_{m=-\infty}^{\infty} \left[\left(\frac{1}{2} - \frac{a_m^+}{\eta_D} \right) \exp\left(-\frac{a_m^+}{\eta_D} \right) + \left(\frac{1}{2} - \frac{a_m^-}{\eta_D} \right) \exp\left(-\frac{a_m^-}{\eta_D} \right) \right] \cdot \sum_{n=-\infty}^{\infty} \left[\exp\left(-\frac{b_n^+}{\eta_D} \right) + \exp\left(-\frac{b_n^-}{\eta_D} \right) \right] \cdot \sum_{j=-\infty}^{\infty} \left[\exp\left(-\frac{c_j^+}{\eta_D} \right) + \exp\left(-\frac{c_j^-}{\eta_D} \right) \right] d\eta_D \quad \text{(B13)}$$

Acknowledgments. This work was supported by the U.S. Nuclear Regulatory Commission under contract NRC-04-97-056 and by the Italian Ministero dell'Universita' e della Ricerca Scientifica e Tecnologica (MURST) 60% "Moto di fluidi e trasporto di inquinanti in formazioni geologiche eterogenee."

References

Aasum, Y., M. G. Kelkar, and S. P. Gupta, An application of geostatistics and fractal geometry for reservoir characterization, *SPE Form. Eval.*, *6*(1), 11–19, 1991.

Ababou, R., and L. W. Gelhar, Self-similar randomness and spectral conditioning: Analysis of scale effect in subsurface hydrology, in *Dynamics of Fluids in Hierarchical Porous Media*, edited by J. H. Cushman, pp. 393–428, Academic, San Diego, Calif., 1990.

Abromwitz, M., and I. A. Stegun, *Handbook of Mathematical Functions*, Dover, Mineola, N. Y., 1972.

Dagan, G., Significance of heterogeneity of evolving scales to transport in porous formations, *Water Resour. Res.*, *30*(12), 3327–3336, 1994.

Desbarats, A. J., and S. Bachu, Geostatistical analysis of aquifer heterogeneity from the core to the basin scale: A case study, *Water Resour. Res.*, *30*(3), 673–684, 1994.

Di Federico, V., and S. P. Neuman, Scaling of random fields by means of truncated power variograms and associated spectra, *Water Resour. Res.*, *33*(5), 1075–1085, 1997.

Di Federico, V., and S. P. Neuman, Flow in multiscale log conductivity fields with truncated power variograms, *Water Resour. Res.*, *34*(5), 975–987, 1998a.

Di Federico, V., and S. P. Neuman, Transport in multiscale log conductivity fields with truncated power variograms, *Water Resour. Res.*, *34*(5), 963–973, 1998b.

Eggleston, J., and S. Rojstaczer, Inferring spatial correlation of hydraulic conductivity from sediment cores and outcrops, *Geophys. Res. Lett.*, *25*(13), 2321–2324, 1998.

Glimm, J., W. B. Lindquist, F. Pereira, and Q. Zhang, A theory of macrodispersion for the scale-up problem, *Transp. Porous Media*, *13*, 97–122, 1993.

Grindrod, P., and M. D. Impey, Fractal field simulations of tracer migration within the WIPP Culebra Dolomite, *Rep. IM2856-1*, vers. 2, 62 pp., Intera Inf. Technol., Denver, Colo., March 1992.

Guzman, A., and S. P. Neuman, Field air injection experiments, in Rasmussen, T. C., Rhodes, S. C., Guzman, A., and Neuman, S. P., *Apache Leap Tuff INTRAVAL Experiments, Results and Lessons Learned*, pp. 52–94, *NUREG/CR-6096*, edited by T. C. Rasmussen et al., U.S. Nucl. Regul. Comm., Washington, D. C., 1996.

Hewett, T. A., Modelling reservoir heterogeneity with fractals, in

Geostatistics Troia, edited by Amilcar Soares, Kluwer Acad., Norwell, Mass., 1992.

Hufschmied, P., Estimation of three-dimensional statistically anisotropic hydraulic conductivity field by means of single well pumping tests combined with flowmeter measurements, in *Proceedings of the International Symposium on the Stochastic Approach to Subsurface Flow*, pp. 110–116, Int. Assoc. for Hydraul. Res., Montvillargenne, France, 1985.

Landau, L. D., and E. M. Lifschitz, *Electrodynamics of Continuous Media*, Pergamon, Tarrytown, N. Y., 1960.

Liu, H. H., and F. J. Molz, Discrimination of fractional Brownian movement and fractional Gaussian noise structures in permeability and related property distribution with range analysis, *Water Resour. Res*., *32*(8), 2601–2605, 1996.

Liu, H. H., and F. J. Molz, Multifractal analysis of hydraulic conductivity distributions, *Water Resour. Res*., *33*(11), 2483–2488, 1997.

Liu, H. H., and F. J. Molz, Comment on "Scaling of random fields by means of truncated power variograms and associated spectra" by V. Di Federico and S. P. Neuman, *Water Resour. Res*., *34*(11), 3207–3208, 1998.

Mandelbrot, B. B., *The Fractal Geometry of Nature*, W. H. Freeman, New York, 1983.

Mandelbrot, B. B., and J. W. Van Ness, Fractional Brownian motions, fractional noises and applications, *SIAM Rev*., *10*, 422–437, 1968.

Molz, F. J., and G. K. Boman, A stochastic interpolation scheme in subsurface hydrology, *Water Resour. Res*., *29*(11), 3769–3774, 1993.

Molz, F. J., and G. K. Boman, Further evidence of fractal structure in hydraulic conductivity distribution, *Geophys. Res. Lett*., *22*(18), 2545–2548, 1995.

Molz, F., H. H. Liu, and J. Szulga, Fractional Brownian motion and fractional Gaussian noise in subsurface hydrology: A review, presentation of fundamental properties, and extensions, *Water Resour. Res*., *33*(10), 2273–2286, 1997.

Molz, F. J., T. A. Hewett, and G. K. Boman, A pseudo-fractal model for hydraulic properties in porous medium, in *Fractals in Soil Sciences*, edited by P. Baveye, J.-Y. Parlange, and B. A. Stewart, pp. 341–372, CRC Press, Boca Raton, Fla., 1998.

Neuman, S. P., Universal scaling of hydraulic conductivities and dispersivities in geologic media, *Water Resour. Res*., *26*(8), 1749–1758, 1990.

Neuman, S. P., Generalized scaling of permeabilities: Validation and effect of support scale, *Geophys. Res. Lett*., *21*(5), 349–352, 1994.

Neuman, S. P., and J. S. Depner, Use of variable-scale pressure test data to estimate the log hydraulic conductivity covariance and dispersivity of fractured granites near Oracle, Arizona, *J. Hydrol*., *102*(1–4), 475–501, 1988.

Neuman, S. P., and V. Di Federico, Correlation, flow and transport in truncated multiscale permeability fields, in *Scale Dependance and Scale Invariance in Hydrology*, edited by G. Sposito, chap. 13, pp. 354–397, Cambridge Univ. Press, New York, 1998.

Painter, S., Evidence for non-Gaussian scaling behavior in heterogeneous sedimentary formations, *Water Resour. Res*., *32*(5), 1183–1195, 1996a.

Painter, S., Stochastic interpolation of aquifer properties using fractional Lévy motion, *Water Resour. Res*., *32*(5), 1323–1332, 1996b.

Perez, G., and M. Kalkar, Assessing distributions of reservoir properties using horizontal well data, in *Reservoir Characterization III*, edited by B. Linville, T. E. Burchfiled, and T. C. Wesson, pp. 399–436, Pennwell, Tulsa, Okla., 1993.

Rajaram, H., and L. W. Gelhar, Plume-scale dependent dispersion in aquifers with a wide range of scales of heterogeneity, *Water Resour. Res*., *31*(10), 2469–2482, 1995.

Robin, M. J. L., E. A. Sudicky, R. W. Gillham, and R. G. Kachanoski, Spatial variability of strontium distribution coefficients and their correlation with hydraulic conductivity in the Canadian forces base Borden aquifer, *Water Resour. Res*., *27*(10), 2619–2632, 1991.

Sudicky, E. A., A natural gradient experiment on solute transport in a sand aquifer: Spatial variability of hydraulic conductivity and its role in the dispersion process, *Water Resour. Res*., *22*(13), 2069–2082, 1986.

Tartakovsky, D. M., Prediction of transient flow in random porous media by conditional moments, Ph.D. dissertation, Dep. of Hydrol. and Water Resour., Univ. of Ariz., Tucson, 1996.

Tartakovsky, D. M., and S. P. Neuman, Transient effective hydraulic conductivities under slowly and rapidly varying mean gradients in bounded three-dimensional random media, *Water Resour. Res*., *34*(1), 21–32, 1998.

Tubman, K. M., and S. D. Crane, Vertical versus horizontal well log variability and application to fractal reservoir modeling, in *Fractals in Petroleum Geology and Earth Processes*, edited by C. C. Barton and P. L. La Pointe, pp. 279–293, Plenum, New York, 1995.

Voss, R. F., Random fractals: Characterization and measurement, in *Scaling Phenomena in Disordered Systems*, edited by R. Pynn and A. Skjeltorp, NATO ASI Ser., *133*, 1985.

Zhan, H., and S. W. Wheatcraft, Macrodispersivity tensor for nonreactive solute transport in isotropic and anisotropic fractal porous media, *Water Resour. Res*., *32*(12), 3461–3473, 1996.

V. Di Federico, DISTART, Università de Bologna, 40136 Bologna, Italy. (vittorio.difederico@mail.ing.unibo.it)

S. P. Neuman, Department of Hydrology and Water Resources, University of Arizona, P.O. Box 210011, Tucson, AZ 85721-0011. (neuman@hwr.arizona.edu)

D. M. Tartakovsky, Group CIC-19, MS B256, Los Alamos National Laboratory, Los Alamos, NM 87545. (dmt@lanl.gov)

(Received November 3, 1998; revised May 17, 1999;
accepted May 17, 1999.)